nature neuroscience

Article

https://doi.org/10.1038/s41593-025-02068-0

Single-dose psilocybin rapidly and sustainably relieves allodynia and anxiodepressive-like behaviors in mouse models of chronic pain

Received: 28 March 2024

Accepted: 20 August 2025

Published online: 2 October 2025

Check for updates

Ahmad Hammo [1], Stephen Wisser [1,2] & Joseph Cichon [1,2]

Chronic pain and mood disorders co-occur, exacerbate one another and share neurobiological mechanisms, but whether a single intervention could promptly alleviate both conditions remains unclear. Here, in two chronic pain models, we show that a single dose of psilocybin induces a rapid and sustained reversal of both mechanical allodynia and anxiodepression-like states in adult male and female mice. Using local psilocin injections, the key active metabolite of psilocybin, we show that the engagement of prefrontal cortical circuits is critical for the concurrent alleviation of both conditions. Two-photon calcium imaging reveals that psilocin rapidly normalizes chronic pain-associated hyperactivity in anterior cingulate cortex layer 2/3 pyramidal neurons. Pharmacologic manipulations with full agonists of 5-HT_{2A} and 5-HT_{1A} receptors replicated some, but not all, of psilocin's cellular and behavioral effects, suggesting that psilocin's actions arise from partial agonism at these receptors within shared circuits governing pain and mood processing.

Chronic pain commonly co-occurs with symptoms of depression and anxiety[1,2]. This comorbidity may compound pain perception, accelerate the transition from acute to chronic pain, discourage patients from following treatment plans and increase risks of prescribed opioid medications[3]. The net effect is associated with greater functional limitations and poorer outcomes[4]. At present, there are limited therapeutic options for managing the co-occurring state[5], but many recognize that the simultaneous assessment and treatment of pain and mood dysfunction is necessary for improved conditions. The convergence of chronic pain and depression involves overlapping dysfunctions in key brain regions, particularly the medial prefrontal cortex (PFC), anterior cingulate cortex (ACC), amygdala and insular cortex[6–8]. In chronic pain, the ACC often shows hyperactivity[9] which has been linked to the affective and attentional dimensions of pain[10]. Hyperactivity is thought to arise from a disrupted excitatory and inhibitory balance, with increased glutamatergic neurotransmission[11], and disinhibition (reduced GABAergic inhibition) amplifying neuronal firing[12]. Additionally, maladaptive synaptic plasticity and enhanced connectivity between the ACC and other pain-related regions, such as the thalamus and insular cortex, contribute to persistent signaling[10]. Furthermore, attenuating ACC neuronal activity via lesions or inactivation techniques relieves aversive responses to pain[13–15]. In depressed patients, the ACC exhibits a heterogeneous activity pattern, exhibiting both hyperactivity and hypoactivity[16,17], reflecting the complexity of the mood state itself and/or its comorbidity with other conditions, such as depressed mood in chronic pain or pain in depression[18]. These neurobiological alterations in the ACC position it as a critical bridge between chronic pain and depression, suggesting that targeting ACC function could offer an integrated therapeutic approach to alleviating symptoms of both conditions.

[1]Department of Anesthesiology and Critical Care, Perelman School of Medicine, University of Pennsylvania, Philadelphia, PA, USA. [2]Department of Neuroscience, Perelman School of Medicine, University of Pennsylvania, Philadelphia, PA, USA. e-mail: joseph.cichon@pennmedicine.upenn.edu

https://doi.org/10.1038/s41593-025-02068-0

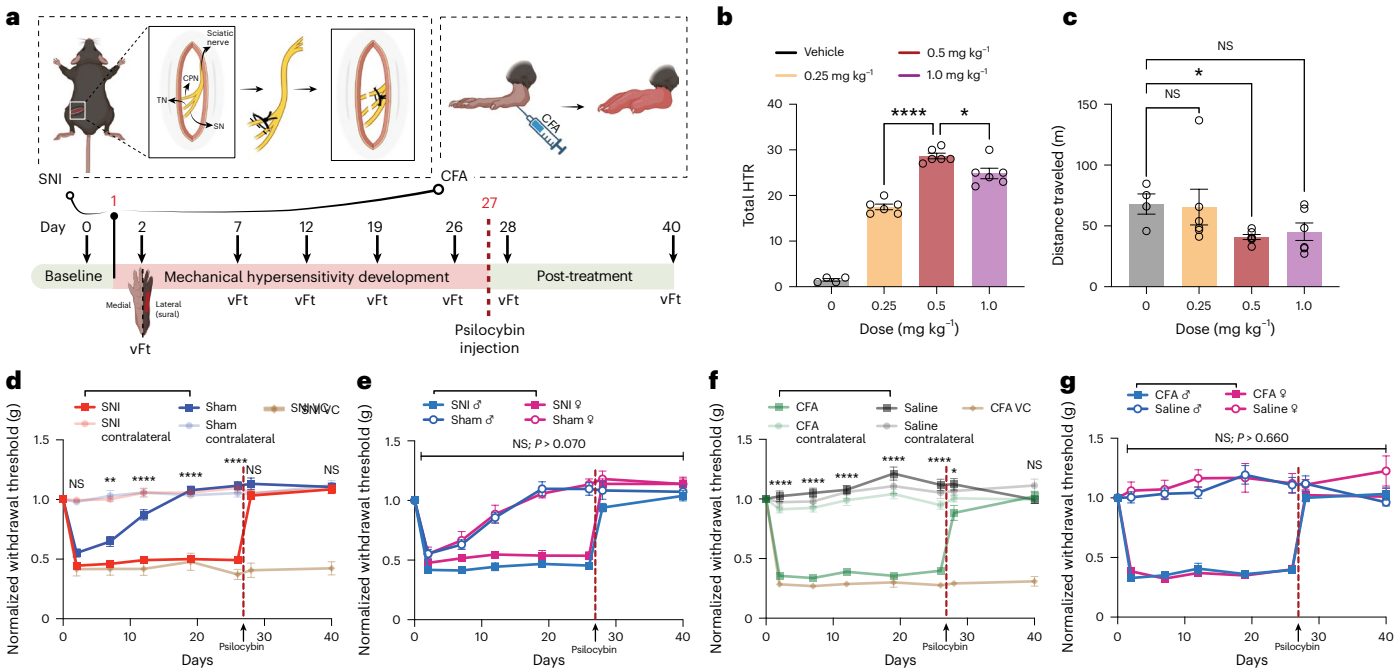

Fig. 1 | A single dose of psilocybin induces rapid and durable reversal of mechanical hypersensitivity in SNI and CFA mice. a, Schematic of experiment timeline. Repeated electronic vF test (vFT, down arrow) was performed before and after pain-inducing interventions (SNI (left) and CFA (right)) and tracked out to 40 days. Psilocybin (red dashed line) injection was performed on day 27. **b**, Total HTR induced by psilocybin following a range of dosing. Moreover, 0.5 mg kg^{-1} dose produced peak HTR over 30 min ($n = 6$) collection window as compared with 0.25 mg kg^{-1} ($n = 6$; one-way analysis of variance, $P < 0.0001$) and 1 mg kg^{-1} ($n = 6$, $P = 0.0153$) dosed animals. **c**, Total distance traveled over 30 min in open field over the same dosing range as in **b**. 0.5 mg kg^{-1} group shows a substantial reduction in total movement compared with vehicle controls (VC) (Kruskal–Wallis (22), $P = 0.047$ followed by Dunn's multiple comparison: $P = 0.048$). **d**,**f**, Normalized hindlimb withdrawal thresholds in SNI (**d**; $n = 30$, $P = 0.00233$ on day 7 and $P < 0.0001$ on days 12, 19 and 26) versus sham ($n = 22$) mice and CFA (**f**; $n = 22$, $P < 0.0001$ on days 2, 7, 12, 19 and 26) versus saline ($n = 15$) mice revealed a persistent state of mechanical hypersensitivity in the affected hindlimb, but not contralateral hindlimb, before treatment. Psilocybin reversed mechanical sensitivity to pre-injury levels on day 28 that persisted for the next 12 days (SNI versus sham, $P > 0.05$ on days 28 and 40; CFA versus saline controls, $P > 0.05$ on days 28 and 40). VC (beige line) indicate no improvement in either SNI (**d**; $n = 6$) or CFA (**f**; $n = 5$) conditions. **e**,**g**, Normalized hindlimb withdrawal threshold separated by sex for SNI/sham (**e**; SNI male, $n = 16$; SNI female, $n = 14$; sham male, $n = 11$; sham female, $n = 11$) and CFA/saline (**g**; CFA male, $n = 11$; CFA female, $n = 11$; saline male, $n = 10$; saline female, $n = 5$) mice. No significant difference in withdrawal thresholds between SNI males and females ($P > 0.05$ on days 2, 7, 12, 19, 26 and 40) or CFA males and females ($P > 0.05$ on days 2, 7, 12, 19, 26, 28 and 40). Data are presented as mean ± s.e.m. Two-way repeated measures analysis of variance in **d**–**g**. ****$P < 0.0001$, **$P < 0.01$, *$P < 0.05$. Detailed statistics are reported in Supplementary Table 1a. TN, tibial nerve; CPN, common peroneal nerve; SN, sciatic nerve; NS, not significant. Panel **a** created with BioRender.com.

Psilocybin, an indole alkaloid, is a naturally occurring psychoactive compound that has been recognized for its analgesic properties since antiquity[19]. Psilocybin itself is pharmacologically inactive but is rapidly converted in the body to its active metabolite, psilocin. Psilocin primarily targets serotonergic receptors, including 5-HT$_{2A}$, 5-HT$_{1A}$ and 5-HT$_{2C}$, where it acts as a partial agonist, mediating its psychoactive and presumed therapeutic effects[20]. More recently, psilocybin and other serotonergic partial agonists have shown early therapeutic promise in managing pain symptoms accompanying chronic neuropathic pain[21–23], cancer pain, psychiatric distress[24], fibromyalgia, migraines and even phantom limb pain[25]. However, psilocybin's effectiveness in treating chronic pain has yet to be rigorously and systematically studied. Moreover, emerging trials suggest psilocybin has rapid and durable therapeutic effects in treatment-resistant depression, anxiety and addiction[26]. Herein, we examine whether a single dose of psilocybin could treat chronic pain and its associated anxiodepressive-like phenotype, using two well-established rodent models of chronic pain.

Results

A single dose of psilocybin relieves chronic neuropathic and inflammatory pain-like states

To produce a chronic pain-like state, we subjected wild-type C57BL/6J mice to either a spared nerve injury (SNI) of the sciatic nerve (sparing the sural nerve) or a single large-volume subcutaneous injection of complete Freund's adjuvant (CFA; consisting of mycobacterial components, ~80–100 µl) to a hindlimb footpad, which model neuropathic and inflammatory pain-like states, respectively[27,28] (Fig. 1a). We opted for a large-volume CFA injection, rather than smaller volumes (10–20 µl)[27,29], to establish a chronic inflammatory pain-like state (Extended Data Fig. 1). The sham conditions for SNI consisted of an incision at the mid-thigh level through the biceps femoris muscle followed by sciatic nerve exposure without nerve manipulation, while CFA controls received a saline injection of equal volume into the hindlimb footpad.

Immediately following SNI or CFA injection, we observed a substantial increase in mechanical hypersensitivity in the affected hindlimb compared with contralateral hindlimb or sham/saline controls, as assessed via repeated electronic von Frey (vF) measurements (Fig. 1d (SNI) and 1f (CFA)). This mechanical hypersensitivity affected both males and females similarly and persisted for 27 days, suggesting a sex-independent chronic state of mechanical allodynia in this preliminary sex-specific analysis (Fig. 1e (SNI) and 1g (CFA)). Once mechanical hypersensitivity stabilized (~4 weeks), mice received a single intraperitoneal injection (i.p.) of psilocybin. A dose–response curve for psilocybin in head-twitch response (HTR) and open field test demonstrated a divergent effect of psilocybin at 0.5 mg kg^{-1} dose, showing peak HTR alongside hypoactivity (Fig. 1b,c and Extended Data Fig. 2). We selected the 0.5 mg kg^{-1} dose for subsequent testing because it produced a maximal effect at a lower dosage as compared with 1 mg kg^{-1}. On the following day (experimental day 28) when animals were reassessed,

https://doi.org/10.1038/s41593-025-02068-0

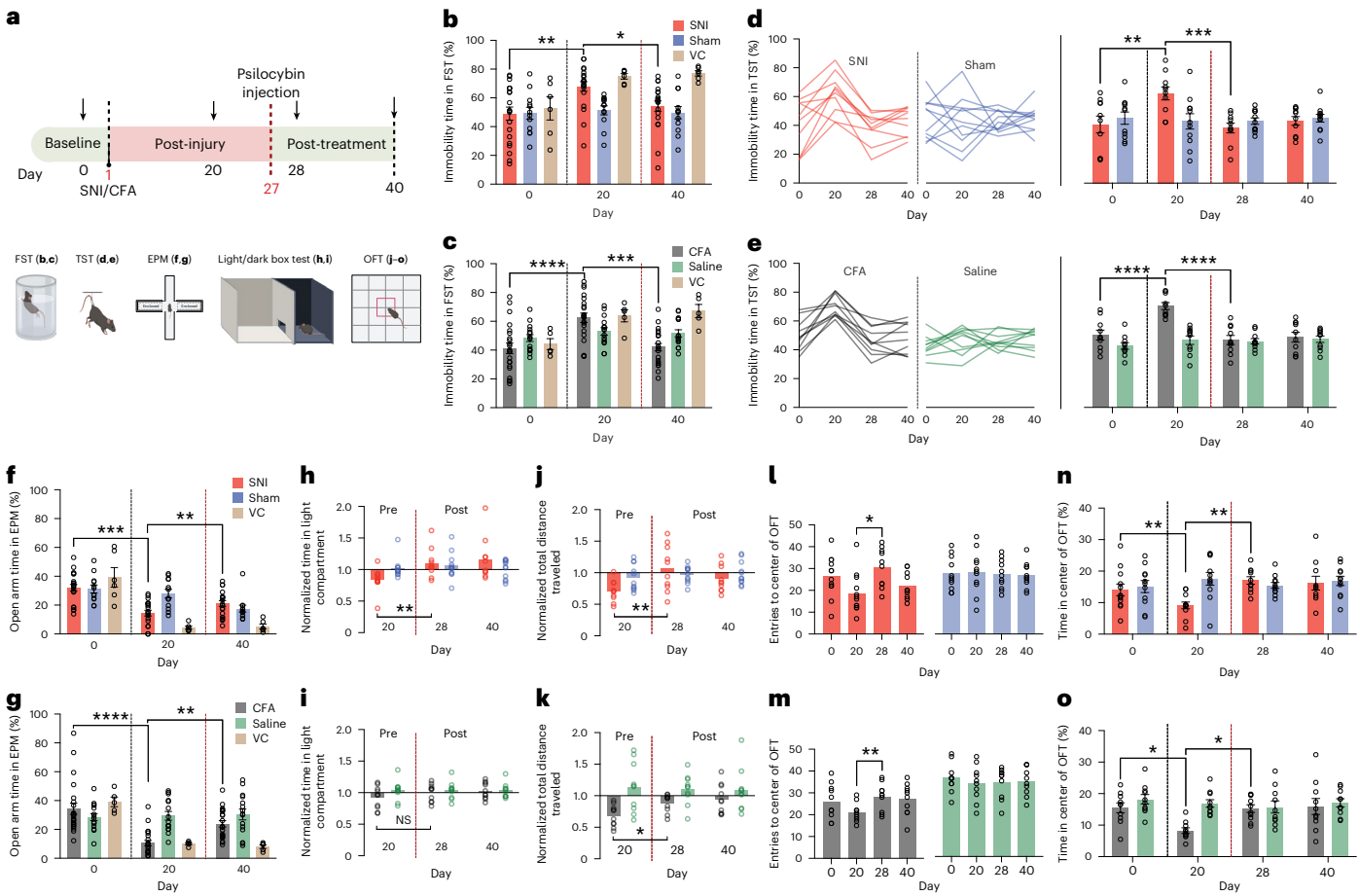

Fig. 2 | Psilocybin reverses anxiodepressive-like behaviors associated with SNI and CFA pain models. a, Experimental timeline for repeated behaviors assessments (down arrow) with FST, TST, EPM, light/dark box test and OFT before intervention (baseline on day 0), 20 days after SNI/CFA interventions, 1 day after psilocybin injection (day 28) and at termination of experiment (day 40). **b**,**c**, SNI (**b**) and CFA (**c**) significantly increased the time spent immobile in FST (SNI, $n = 20$, $P = 0.00487$; CFA, $n = 22$, $P = 8.7 \times 10^{-5}$), which was later decreased by psilocybin (SNI, $P = 0.042$; CFA, $P = 0.00011$). **d**,**e**, Individual animal performance in TST (left) and summary (right) for SNI (**d**)/CFA (**e**) and sham (**d**)/saline (**e**) controls. Immobility time increased postinjury (SNI, $P = 0.00267$; CFA, $P < 0.0001$) and decreased after psilocybin treatment (SNI, $P = 0.00066$; CFA, $P < 0.0001$). **f**,**g**, Percentage of time spent in the open arm of the EPM in SNI ($n = 20$), sham ($n = 12$) and VC ($n = 5$; **f**) and CFA ($n = 22$), saline ($n = 15$) and VC ($n = 5$; **g**) mice. SNI/CFA induced a significant decrease (SNI, $P = 0.00019$; CFA, $P = 6.6 \times 10^{-7}$) in open arm time which was reversed by psilocybin administration (SNI, $P = 0.0095$; CFA, $P = 0.0022$). No improvement was observed in VCs (SNI, $P > 0.999$; CFA, $P > 0.999$). **h**,**i**, Normalized total time spent in the light compartment of the light/dark test (baseline, day 0). Time in light compartment decreases postinjury (SNI, $n = 10$; CFA, $n = 10$) but returns to pre-injury levels after psilocybin injection in SNI (**h**) but not in CFA (**i**) mice (SNI, $P = 0.0099$; CFA, $P > 0.999$). **j**–**o**, SNI and CFA animals also exhibited reduced total distance traveled (**j**; SNI, $n = 10$; **k**; CFA, $n = 10$), entries to the center (**l**; SNI, $P = 0.292$; **m**; CFA, $P = 0.051$) and time spent in the center area (**n**; SNI, $P = 0.0027$; **o**; CFA, $P = 0.011$) in OFT. SNI/CFA after psilocybin treatment increased in total distance traveled (**j**; SNI, $P = 0.0021$; **k**; CFA, $P = 0.0458$), entries to the center (**l**; SNI, $P = 0.0295$; **m**; CFA, $P = 0.00178$) and time spent in the central area (**n**; SNI, $P = 0.0053$; **o**; CFA, $P = 0.0161$). Behavioral changes persisted until day 40, whereas the control groups remained unchanged over repetitive testing intervals. Data are represented as mean ± s.e.m. $^{****}P < 0.0001$, $^{***}P < 0.001$, $^{**}P < 0.01$, $^{*}P < 0.05$. Detailed statistics are reported in Supplementary Table 1b. Panel **a** created with BioRender.com.

we detected a complete reversal of mechanical hypersensitivity in both SNI and CFA animals (Fig. 1d,e (SNI) and 1f,g (CFA)). This restorative effect induced by psilocybin persisted in both sexes of SNI and CFA animals for a minimum of 12 days, marking the experiment's endpoint. These results suggest that a single dose of psilocybin induces a rapid and durable analgesic effect in two distinct conditions associated with chronic pain.

Psilocybin alleviates mood changes associated with chronic neuropathic and inflammatory pain-like states

We next assessed whether SNI- and CFA-induced mechanical allodynia was associated with co-occurring anxiodepressive-like behaviors. Trends in anxiety-related behavior were made by tracking animal's performance in the elevated plus maze (EPM), open field test (OFT) and light/dark box test, while behavioral despair was assessed in the forced swim test (FST) and tail suspension test (TST) before and after SNI/CFA procedures (Fig. 2a). Consistent with chronic pain-like states driving robust affective changes in preclinical models[8], both SNI and CFA mice displayed substantial changes in both depression and anxiety associated assays compared with sham/saline controls on day 20 (Fig. 2b–e (depression testing) and 2f–o (anxiety testing)). Within SNI and CFA mice, we did not observe any substantial sex-specific differences across FST, TST, EPM, light/dark box, or OFT (Extended Data Fig. 3). These behavioral shifts were accompanied by deficits in motor skill performance, as evidenced by reduced latency to fall on an accelerating rotarod test, suggesting either fatigue or impaired motor performance related to the behavioral state (allodynia and/or anxiodepressive-like behaviors; Extended Data Fig. 4). Collectively, these results indicate that SNI/CFA-induced chronic mechanical hypersensitivity contributes to the emergence of affective disturbances, including features consistent with behavioral despair, anxiety-like behaviors and impaired motor skill performance.

https://doi.org/10.1038/s41593-025-02068-0

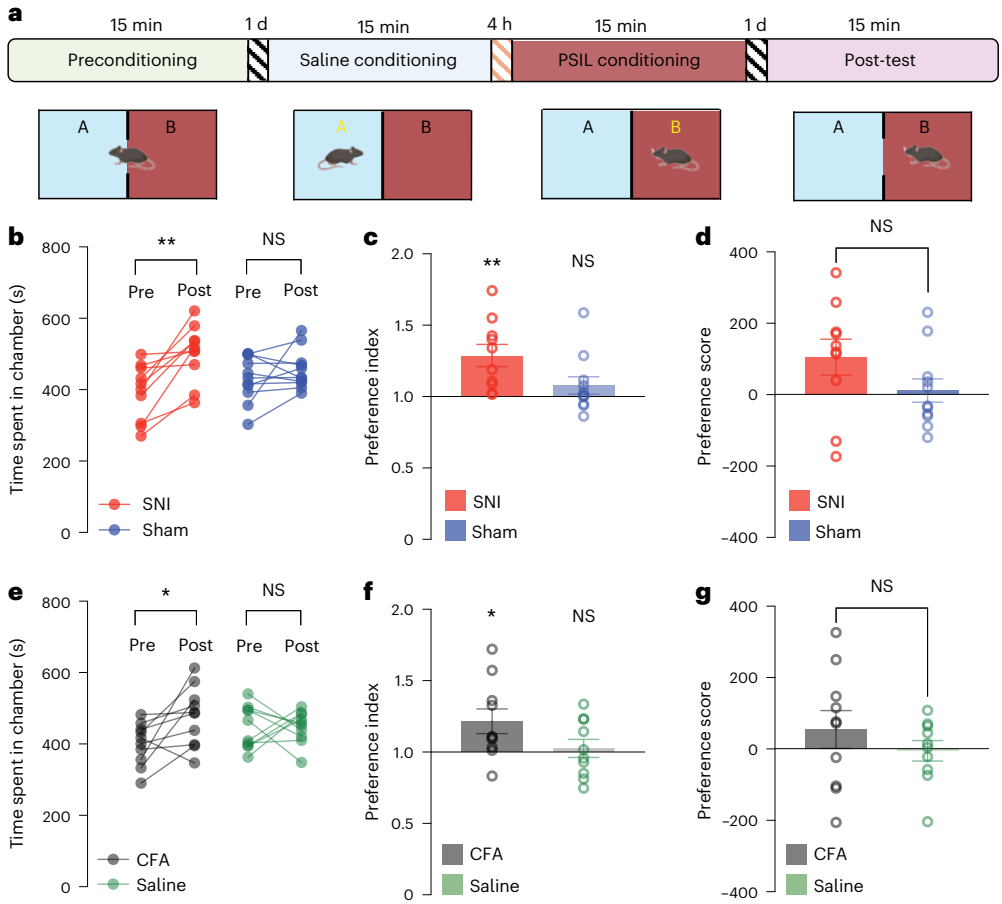

Fig. 3 | Psilocybin promotes preference for the treatment chamber in the CPP test. a, Experimental timeline for CPP test for psilocybin versus saline on day 27 in SNI/CFA mice. **b**,**e**, Total time spent in chamber B (psilocybin-paired chamber) increases following psilocybin injection in SNI (**b**) and CFA (**e**) mice (SNI, $n = 10$, $P = 0.0022$; CFA, $n = 10$, $P = 0.0198$) but remains unchanged in sham (**b**) and saline (**e**) mice following saline injection. **c**,**f**, SNI (**c**) and CFA (**f**) mice increase preference (index represents the ratio of time spent in chamber B between post-test and pretest periods) for the treatment chamber (SNI, $P = 0.0047$; CFA, $P = 0.0341$). **d**,**g**, SNI (**d**) and CFA (**g**) mice have greater preference scores (which represent the total difference in time spent in chamber B versus chamber A post-test) for the treatment chamber compared with sham (**d**) and saline (**g**) mice. Data are represented as mean ± s.e.m. $^{**}P < 0.01$, $^{*}P < 0.05$. Detailed statistics are reported in Supplementary Table 1c. PSIL, psilocybin.

To determine if these SNI/CFA-induced anxiodepressive-like behaviors could be cotreated by psilocybin, mice received a single dose of psilocybin on day 27, followed by repeat behavioral testing. Here we found that psilocybin treatment substantially reversed SNI/CFA-induced affective-related behaviors and motor function deficits, while sham/saline controls remained unaffected (Fig. 2 and Extended Data Fig. 4). The normalization of mechanical sensitivity in both SNI and CFA mice paralleled an increase in open-arm activity in EPM and mobility in FST (Extended Data Fig. 5). Examination of the surgical site in SNI mice treated with psilocybin revealed the presence of a neuroma—an anticipated consequence of common peroneal nerve and tibial nerve transection (Extended Data Fig. 6). This finding suggests that psilocybin-induced reversal of behavioral outcomes is unlikely to result from peripheral nerve regeneration within the post-treatment timeframe. Taken together, these experiments suggest that psilocybin acts as a multimodal therapeutic agent, inducing both analgesic and antidepressant/anti-anxiety-like effects following a single treatment.

SNI and CFA animals show preference for psilocybin treatment

To assess whether psilocybin elicited analgesic effects independent of mechanical testing, we subjected SNI/CFA mice to a conditioned place preference (CPP) paradigm (Fig. 3a). On day 27, animals were preconditioned to a two-chamber apparatus, where baseline preferences were established by allowing free exploration of both chambers without any interventions. Following this, mice were conditioned over the next day by receiving saline injections paired with one chamber ('A') and psilocybin injections (0.5 mg kg^{-1} i.p.) paired with the opposite chamber ('B'). Each conditioning session was conducted with the mice confined to the respective chamber for 15 min immediately following injection. Following the conditioning phase, a post-testing session was conducted, during which mice were allowed to freely explore both chambers without any further drug administration. The time spent in each chamber during post-testing was recorded to assess the development of a conditioned preference for a particular chamber. Consistent with psilocybin driving an analgesic state, both SNI and CFA mice treated with psilocybin exhibited a substantial increase in time spent in the psilocybin-paired chamber (chamber 'B'; Fig. 3b,d). Sham or saline controls failed to show a preference for psilocybin. This behavior, reflected in the preference index (Fig. 3c for SNI/sham and 3e for CFA/saline), indicates that psilocybin's alleviation of mechanical allodynia (Fig. 1) fosters a positive behavioral association for the environment associated with analgesia. This effect also aligns with observed improvements in anxiodepressive-like behaviors (Fig. 2), highlighting the interconnected nature of the analgesic state and improved mood changes.

https://doi.org/10.1038/s41593-025-02068-0

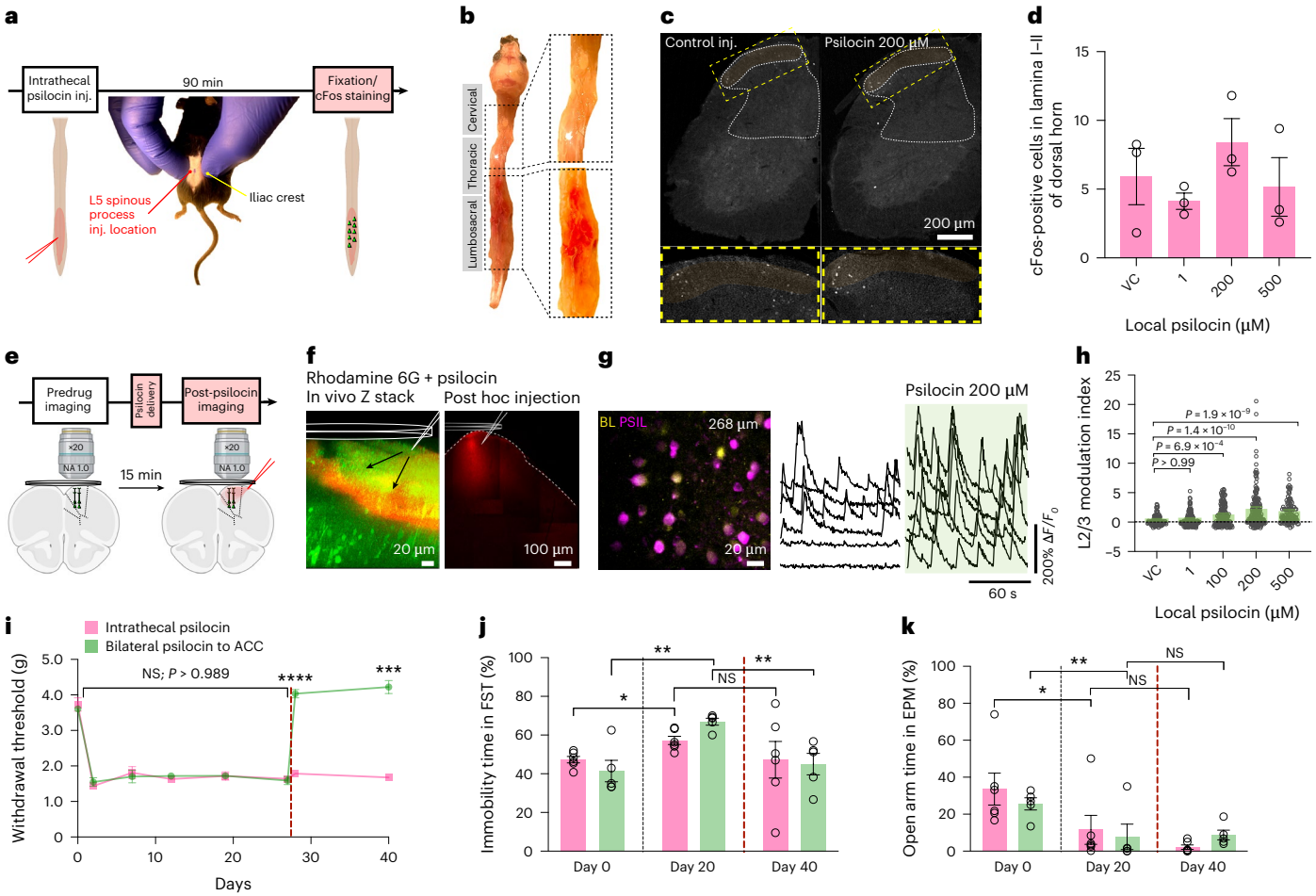

Fig. 4 | Local application of psilocin to the ACC reverses SNI-induced mechanical allodynia and anxiodepressive-like behaviors. a, Experimental timeline of intrathecal injection (inj.) of psilocin to the lumbosacral region of the spinal cord followed by cFos immunostaining. Photograph (middle) shows the animal's positioning and targeting of the lower lumbar region for single-shot delivery of psilocin mixed with Rhodamine 6G. **b**, Extracted spinal column from animal receiving psilocin/Rhodamine 6G demonstrates vertical tracking of the mixture within the intrathecal space. **c**, Representative confocal images of the lumbosacral dorsal horn (white dashed line) from animals treated with either saline or psilocin (200 µM). Lamina I–II shown in yellow dashed boxes. **d**, Summary of c-Fos expression induced by differing concentrations of psilocin (1, 200 and 500 µM; $n = 3$ animals per condition) compared with VCs. **e**, Schematic illustrating the experimental approach for delivering local psilocin to the ACC. Psilocin was combined with Rhodamine 6G to track its spread through living tissue. **f**, Real-time two-photon Z-stack (left) and post hoc confocal images (right) following injection of psilocin mixed with Rhodamine 6G demonstrate localized cortical application. **g**, Left: two-photon time-lapse recordings (2 min) shown as a maximum projection with wakefulness (yellow) and local psilocin (200 µM) application (magenta) overlaid. Right: representative GCaMP6f traces of individual neurons under wakefulness and following local psilocin. **h**, Summary of L2/3 neuronal activity across escalating local psilocin doses (VC, 108 neurons from 3 mice; 1 µM, 175 neurons from 4 mice; 100 µM, 170 neurons from 3 mice; 200 µM, 179 neurons from 3 mice; 500 µM, 113 neurons from 3 mice). One-sided Kruskal–Wallis (88), $P = 2.6 \times 10^{-18}$ followed by Dunn's multiple comparison, L-psilocin at concentrations >100 µM, $P < 0.001$ as compared with 1 µM, $P > 0.99$. Exact P values are shown in the figure. **i**, Serial withdrawal threshold responses revealed bilateral psilocin to ACC ($n = 5$) induced rapid and sustained analgesic effects as compared with intrathecal psilocin ($n = 6$; day 28, $P = 1.7 \times 10^{-5}$; day 40, $P = 0.0001$). **j**,**k**, Bilateral psilocin to ACC failed to improve EPM open activity (**k**; EPM (17.6), $P = 0.004$ followed by Dunn's comparisons: ACC day 20 versus day 40, $P = 0.99$; intrathecal day 20 versus day 40, $P = 0.99$) but reduced FST immobility time (**j**; FST (14.8), $P = 0.01$ followed by Dunn's comparisons: ACC day 20 versus day 40, $P = 0.009$; intrathecal day 20 versus day 40, $P = 0.99$). Data are presented as mean ± s.e.m. ****$P < 0.0001$, ***$P < 0.001$, **$P < 0.01$, *$P < 0.05$. Detailed statistics are reported in Supplementary Table 1d. BL, baseline. Panel **a** created with BioRender.com.

Local application of psilocin to the ACC is sufficient for the rapid restorative effect of SNI-induced mechanical allodynia and anxiodepressive-like behaviors

The simultaneous reduction of mechanical allodynia (Fig. 1) and anxiodepressive-like behaviors (Fig. 2) could arise at multiple locations along the neuraxis[30–32]. To further pinpoint the critical cohort of presumed serotonergic receptors and circuits mediating psilocybin's therapeutic effects, we locally administered psilocin, the active metabolite of psilocybin produced following hepatic dephosphorylation, either to the lumbosacral region of the spinal cord or bilaterally to the ACC on day 27 (Fig. 4a,e). Given that the intact sural nerve, primarily deriving its sensory fibers from L4 to S2, becomes hypersensitive following SNI, we specifically targeted psilocin to this region via a single intrathecal injection (Fig. 4a). At both injection locations, psilocin was co-injected with Rhodamine 6G to visualize its presence and local spread within the respective regions (Fig. 4b,f). A dose–response curve of intrathecal psilocin (vehicle control–1, 200 and 500 µM; ~5 µl total) revealed a dose of 200 µM increased the immediate early gene cFos expression, a slow integrator of neuronal activity, in dorsal horn lamina I–II of the lumbosacral spinal cord (Fig. 4c,d). Similarly, local application of psilocin to the ACC region (vehicle control–1, 100, 200, 500 µM; ~2 µl total), assessed using two-photon calcium imaging of pyramidal neurons in awake head-fixed mice expressing GCaMP6f under the CaMK-II promoter, revealed a progressive spontaneous

https://doi.org/10.1038/s41593-025-02068-0

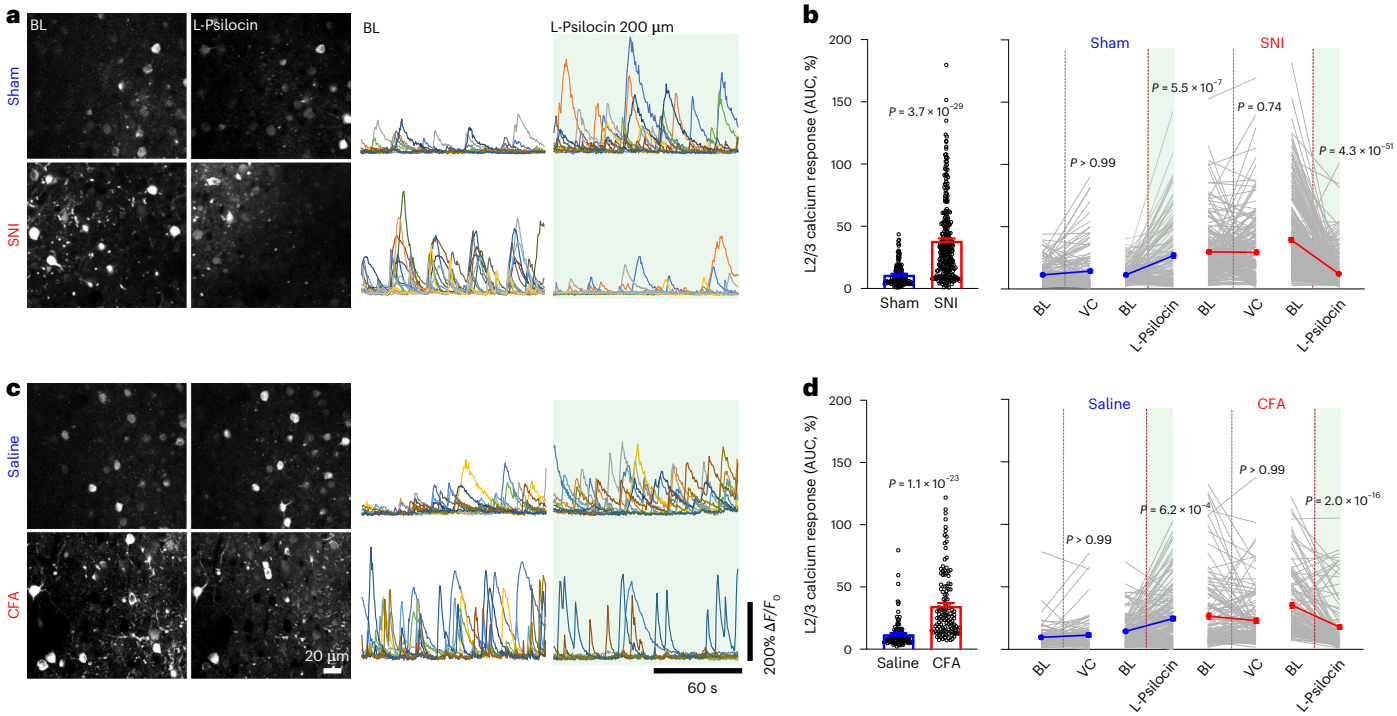

Fig. 5 | Local psilocin normalizes the spontaneous hyperactivity of pyramidal neurons in both neuropathic and inflammatory pain states. a,**c**, Two-photon max projection images (left) and GCaMP6f fluorescence traces (right; different cells shown in different colors) of 2-min recording from L2/3 neurons of ACC in sham (**a**)/saline (**c**) (top) and SNI (**a**)/CFA (**c**) mice (bottom). Of note, SNI/CFA procedure induces spontaneous hyperactivity as compared with sham/saline animals. Local (L-) cortical application of psilocin (200 µM) induces divergent effects on neuronal activity—an activation of L2/3 neurons in control mice, whereas L2/3 neuronal activity suppression in SNI/CFA mice. **b**,**d**, Left: average integrated calcium activity over 2 min in L2/3 neurons 3 weeks post-SNI (**b**; SNI, 38.3 ± 1.9, n = 275 cells from 4 mice; sham, 11.1 ± 0.8, n = 143 cells from 3 mice; two-tailed Mann–Whitney test (6528), $P = 3.7 \times 10^{-29}$) and CFA (**d**; CFA, 34.8 ± 2.3, n = 126 cells from 3 mice; saline control, 12.0 ± 1.0, n = 123 cells from 3 mice; two-tailed Mann–Whitney test (2,049), $P = 1.1 \times 10^{-23}$). Right: summary of L2/3 calcium responses in control and SNI/CFA mice before and after local cortical application of vehicle (saline) or psilocin (200 µM; light green-shaded area). Of note, the substantial suppression of L2/3 activity in SNI/CFA mice following psilocin application (SNI—one-sided Kruskal–Wallis (384), $P = 6.9 \times 10^{-79}$ followed by Dunn's multiple comparison. L-Psilocin ($P < 0.001$) significantly suppressed activity in both sham (143 neurons from 3 mice) and SNI (275 neurons from 4 mice) mice, whereas VC ($P > 0.99$) had no effect in sham (143 neurons from 3 mice) and SNI mice (194 neurons from 3 mice). CFA—one-sided Kruskal–Wallis (165), $P = 2.5 \times 10^{-32}$ followed by Dunn's multiple comparison. L-Psilocin ($P < 0.001$) significantly suppressed activity in both saline control (166 neurons from 3 mice) and CFA (126 neurons from 3 mice) mice, whereas VC ($P > 0.99$) had no effect in both saline (82 neurons from 3 mice) and CFA mice (132 neurons from 3 mice)). Exact P values are shown in the figure. Error bars show s.e.m. AUC, area under the curve.

recruitment of layer 2/3 (L2/3) pyramidal neurons with peak activity at a dose of ~200 µM over baseline measurements (Fig. 4g,h and Extended Data Fig. 7). Given the inverted U-shaped response observed in these experiments, we reasoned that the 200 µM dose might effectively engage local postsynaptic serotonergic receptor signaling to modulate neuronal activity involved in pain processing.

Next, we evaluated whether the local application of psilocin to the ACC or the intrathecal space of the lumbosacral spinal cord in SNI mice would be sufficient to drive the simultaneous restorative effect of mechanical hypersensitivity and associated anxiodepressive-like behaviors. SNI mice receiving bilateral psilocin injections experienced a rapid and persistent reversal of mechanical hypersensitivity when assessed on day 28, lasting until day 40 (Fig. 4i). When the same mice were tested for anxiodepressive-like changes, we observed a substantial improvement in the FST, marked by a decrease in immobile time (Fig. 4j). However, we observed no improvement in time spent on the open arm in EPM compared with prepsilocin treatment measurements (Fig. 4k). In contrast, mice treated with intrathecal psilocin showed persistent allodynia, with no substantial changes in withdrawal thresholds (Fig. 4i). These same mice also exhibited no substantial changes in either EPM or FST behaviors (Fig. 4j,k). Taken together, these results suggest that psilocin's effects on mechanical hypersensitivity and mood-related dysfunction are likely mediated by supraspinal circuits, with the ACC having a key role.

Local psilocin normalizes spontaneous hyperactivity of pyramidal neurons in both neuropathic and inflammatory pain-like states

To investigate how local application of psilocin to the ACC might reverse these behaviors, we used two-photon calcium imaging in awake, head-restrained SNI/CFA and control mice expressing GCaMP6f in pyramidal neurons after establishing chronic pain-like states. In SNI/CFA mice, L2/3 pyramidal neurons exhibited a substantial elevation in spontaneous activity as compared with sham and saline-injected controls (Fig. 5a,c). Due to the sustained nature of these transients, we quantified calcium activity as the area under the curve of the $\Delta F/F_0$ trace for individual neurons, capturing changes in both frequency and amplitude. On day 20, SNI and CFA mice displayed comparable levels (Mann–Whitney test, $P = 0.70$) of heightened neuronal activity, suggesting neuropathic and inflammatory pain signals similarly converge and restructure ACC neuronal activity into a hyperactive state (Fig. 5b,d (left)). Remarkably, local psilocin application (200 µM; ~2 µl total) rapidly suppressed (SNI, −38 ± 5.8%; CFA, −44 ± 4.8%) the SNI/CFA-associated hyperactivity to control levels (Fig. 5a–d). SNI/CFA mice receiving vehicle controls showed persistent hyperactivity (Fig. 5b,d). This psilocin-induced reconfiguration of L2/3 neuronal activity was unexpected, as psilocin induced an activating effect in control wild-type mice in Fig. 4h and sham/saline controls in Fig. 5a,c (top). We hypothesize that psilocin's capacity to suppress

https://doi.org/10.1038/s41593-025-02068-0

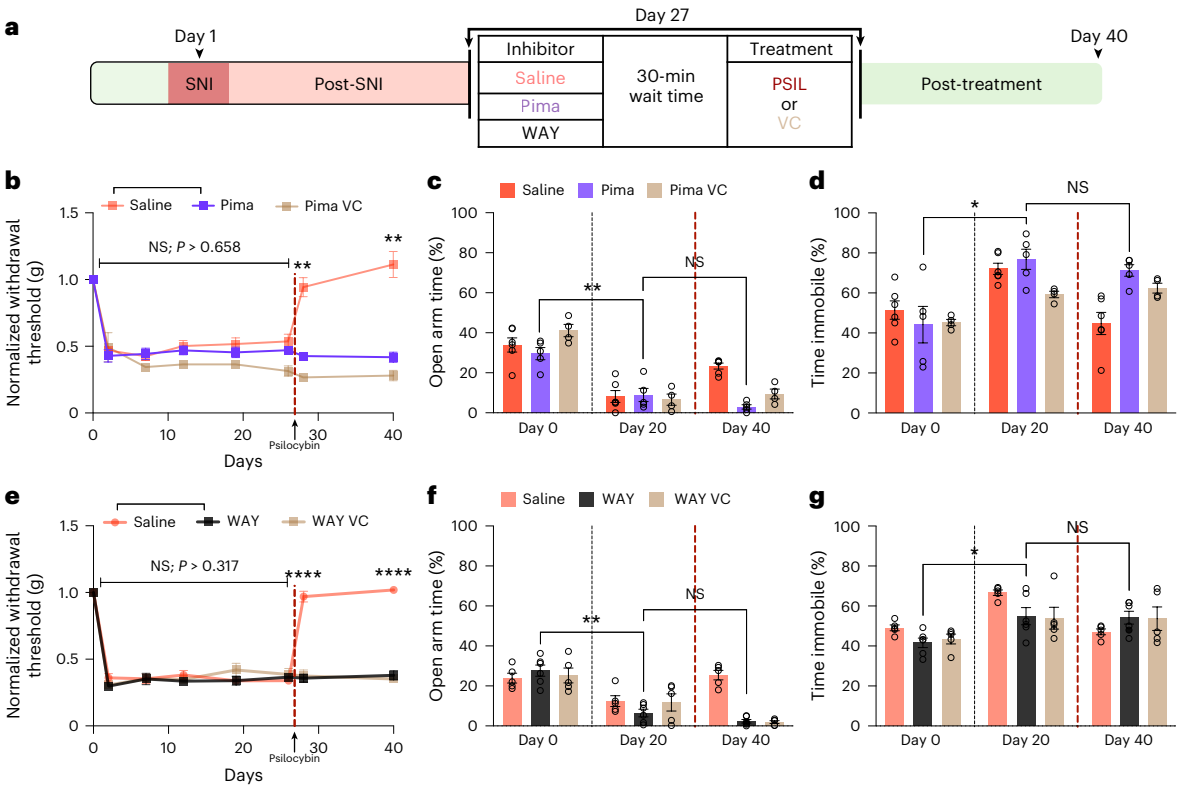

Fig. 6 | Activation of both 5-HT$_{1A}$ and 5-HT$_{2A}$ receptors is necessary for psilocybin's reversal of SNI-induced mechanical hypersensitivity and anxiodepressive-like behaviors. a, Experimental timeline of 5-HT$_{1A}$ (WAY) and 5-HT$_{2A}$ (Pima) receptor blockade before PSIL or VC injection in SNI mice. **b**, Normalized hindlimb withdrawal thresholds in saline ($n = 5$), Pima ($n = 5$) or Pima VC ($n = 4$) groups. Pima blocks the restorative effect of psilocybin on mechanical hypersensitivity compared with saline-injected mice ($P = 0.003$ on day 28 and day 40). **c**,**d**, Pima blocks psilocybin-induced increase in EPM open arm time (**c**; $n = 5$, $P > 0.999$) and decrease in FST immobile time (**d**; $n = 5$, $P > 0.999$). Similar trends were observed in mice receiving Pima followed by VC injection. **e**, Normalized hindlimb withdrawal thresholds in saline ($n = 5$), WAY ($n = 6$) or WAY VC ($n = 5$) groups. WAY blocks psilocybin-induced changes in mechanical hypersensitivity compared with saline mice ($P < 0.0001$ on day 28 and day 40). **f**,**g**, WAY also blocks psilocybin-induced increases in EPM open arm time (**f**; $n = 5$, $P > 0.05$) and decreases in FST immobile time (**g**; $n = 5$, $P > 0.05$). WAY followed by VC injection showed no changes. Data are presented as mean ± s.e.m. ****$P < 0.0001$, ***$P < 0.001$, **$P < 0.01$, *$P < 0.05$. Detailed statistics are reported in Supplementary Table 1f. Pima, pimavanserin; WAY, WAY-100635.

neuronal hyperactivity in the ACC may stem from its multifaceted pharmacological actions on postsynaptic serotonergic receptors expressed by cortical neurons.

Both 5-HT$_{2A}$ and 5-HT$_{1A}$ receptor signaling is necessary for psilocybin's restorative effect on mechanical hypersensitivity and anxiodepressive-like behaviors

To evaluate whether psilocin's suppression of neuronal activity is related to activation of a specific serotonergic receptor subtype, we subjected SNI mice to either 5-HT$_{2A}$ or 5-HT$_{1A}$ receptor blockade before systemic psilocybin administration (Fig. 6a). Here SNI mice on day 27 were given either pimavanserin (1 mg kg^{-1} i.p. dose), a 5-HT$_{2A}$ receptor inverse agonist[33] or WAY-100635 (1 mg kg^{-1} i.p. dose), a selective 5-HT$_{1A}$ antagonist[34], 30 min before receiving psilocybin (0.5 mg kg^{-1}). Pimavanserin pretreatment occluded the spontaneous generation of psilocybin-induced head twitches and its rapid analgesic effects, as withdrawal thresholds remained persistently low on day 28 (Fig. 6b and Extended Data Fig. 8). Similarly, pretreatment with WAY-100635 also prevented psilocybin's reduction of mechanical hypersensitivity (Fig. 6e). Furthermore, the blockade induced by either pimavanserin or WAY-100635 persisted for up to 40 days, indicating that both antagonists also abolished psilocybin's long-lasting effects (Fig. 6b,e).

When tested in the EPM and FST, both inhibitors blocked psilocybin's anti-anxiety and antidepressant-like effects (Fig. 6c,d,f,g). Time spent on the open arms of the EPM decreased in both groups (Fig. 6c,f), while time spent immobile in the FST remained higher compared with baseline levels (Fig. 6d,g). Control mice injected with saline of equal volume 30 min before psilocybin still received the full therapeutic effect in all behavior assays (Fig. 6b–g). Mice receiving only inhibitors (vehicle controls) showed no improvement in any behavioral assays (Fig. 6b–g). Taken together, psilocybin's rapid and long-lasting analgesic effects are tied to its immediate pharmacological action that depends on initial receptor activation—5-HT$_{2A}$ targeted by pimavanserin and 5-HT$_{1A}$ targeted by WAY-100635. Since blocking these receptors at the time of administration prevented prolonged analgesia, this suggests that psilocybin's therapeutic effects require specific serotonergic receptor engagement during its acute phase to initiate long-term changes.

Therapeutic effect of psilocybin partially replicated by pharmacologically induced full agonism of 5-HT$_{2A}$ and 5-HT$_{1A}$ receptors

The blockade of psilocybin-induced improvements in mechanical hypersensitivity and affective behaviors by 5-HT$_{2A}$ and 5-HT$_{1A}$ receptor antagonists suggests that activation of both receptor types is necessary to mediate these effects. To this end, we first explored the effect of 5-HT$_{2A}$ and 5-HT$_{1A}$ receptor activation on cortical neuronal activity induced by local application of either the phenylalkylamine 2,5-dimethoxy-4-iodoamphetamine (DOI), 5-HT$_{2A}$ receptor full agonist or 8-hydroxy-2-(di-n-propylamino)tetralin (8-OH-DPAT), a 5-HT$_{1A}$ receptor full agonist. Calcium imaging of L2/3 neurons before and after DOI revealed that DOI induced a strong activation of neuronal activity in both SNI (44% increase) and sham (93% increase) mice (Fig. 7a,b).

https://doi.org/10.1038/s41593-025-02068-0

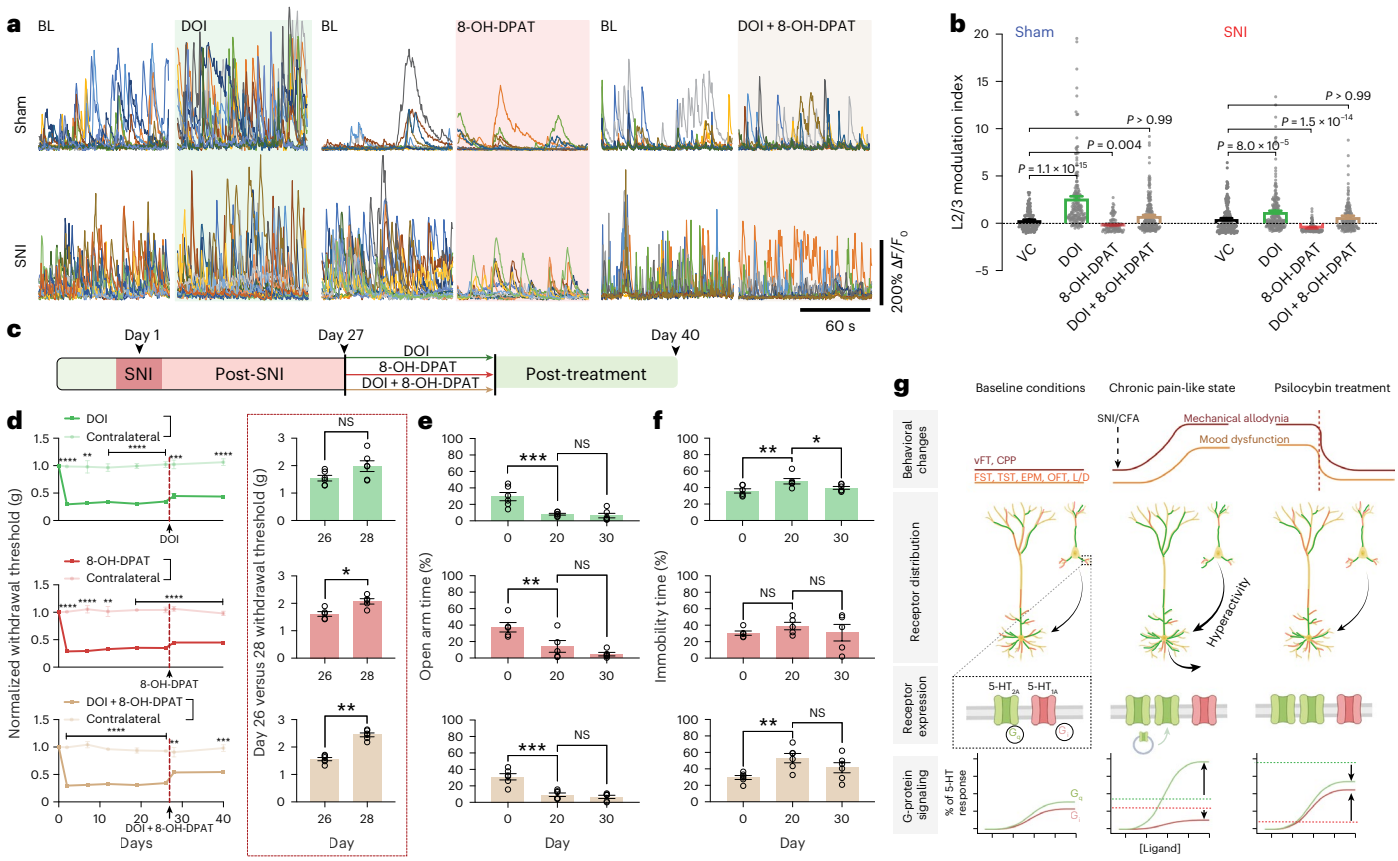

Fig. 7 | Partial reduction of mechanical hypersensitivity by pharmacologically induced full agonism of 5-HT$_{2A}$ and 5-HT$_{1A}$ receptors. a, Representative GCaMP6f fluorescence traces from an ACC cortical region (different cells shown in different colors) in sham and SNI mice before and after local application of DOI (sham, $n = 189$ neurons from 4 mice; SNI, $n = 222$ neurons from 4 mice), 8-OH-DPAT (sham, $n = 101$ neurons from 3 mice; SNI, $n = 126$ neurons from 3 mice) or DOI + 8-OH-DPAT (sham, $n = 224$ neurons from 5 mice; SNI, $n = 171$ neurons from 5 mice). **b**, Summary of L2/3 neuronal activity across different drug conditions. Please note the substantial activation induced by DOI, suppression induced by 8-OH-DPAT and normalizing effect of DOI + 8-OH-DPAT (one-sided Kruskal–Wallis (324), $P = 3.5 \times 10^{-66}$ followed by Dunn's multiple comparison. DOI or 8-OH-DPAT alone, $P < 0.01$ for both sham and SNI mice, whereas DOI + 8-OH-DPAT, $P > 0.99$ in sham and SNI mice). **c**, Experimental timeline of DOI, 8-OH-DPAT or DOI + 8-OH-DPAT injection in SNI mice on day 27. **d**, Left: normalized hindlimb withdrawal thresholds (g) in SNI mice treated with DOI ($n = 6$), 8-OH-DPAT ($n = 5$) or DOI + 8-OH-DPAT on day 27 ($n = 6$). Agonists fail to restore withdrawal thresholds back to contralateral hindlimb levels (day 28—DOI, $P = 0.002$; 8-OH-DPAT; $P < 0.0001$; DOI + 8-OH-DPAT, $P = 0.0069$). Right: day 26 versus day 28 indicates significant improvements in withdrawal thresholds 1-day post-8-OH-DPAT injection ($P = 0.0159$) and DOI + 8-OH-DPAT injection ($P = 0.0022$); however, no significant effect is observed in the DOI group ($P = 0.0931$). **e**, EPM open arm time pre-injury, postinjury and post-treatment. No significant improvement was observed postinjection across all drug groups (DOI, $P > 0.999$; 8-OH-DPAT, $P = 0.1639$; DOI + 8-OH-DPAT, $P = 0.9612$). **f**, TST immobility time pre-injury, postinjury and post-treatment. DOI induced a significant reduction in immobility time (DOI, $P = 0.0285$), while 8-OH-DPAT ($P = 0.7145$) and DOI + 8-OH-DPAT ($P = 0.117$) induced no significant changes. **g**, Working model of psilocybin's rapid rescue of mechanical allodynia and mood dysfunction. Neuropathic and inflammatory pain states induce molecular and cellular changes that result in ACC hyperexcitability and spontaneous hyperactivity. 5-HT$_{2A}$ receptor upregulation and 5-HT$_{1A}$ downregulation (or their coupling/signaling) in the chronic pain state may contribute to these cellular maladaptations. The psilocin-induced partial agonism at these postsynaptic receptors could serve to rebalance G-protein coupling/signaling to suppress ACC hyperactive neurons contributing to the normalization of mechanical allodynia and mood dysfunction. Data are presented as mean ± s.e.m. ****$P < 0.0001$, ***$P < 0.001$, **$P < 0.01$, *$P < 0.05$. Detailed statistics are reported in Supplementary Table 1g. L/D, light/dark box test. Panel **g** created with BioRender.com.

Conversely, 8-OH-DPAT caused a reduction in neuronal activity in both SNI (64% decrease) and sham (25% decrease) mice (Fig. 7a,b). The combined local application of DOI and 8-OH-DPAT produced an intermediate effect in both SNI (22% increase) and sham (2.8% decrease) mice relative to the perturbations induced by each drug alone (Fig. 7a,b).

To determine if these local serotonergic-induced changes in L2/3 neuronal activity might relate to the psilocybin-induced analgesic state and associated anxiodepressive-like behaviors, we pharmacologically agonized the same cohorts serotonergic receptors in four treatment groups in SNI mice—5-HT$_{1A}$ with 8-OH-DPAT (1 mg kg^{-1} i.p.), 5-HT$_{2A}$ with DOI (0.5 mg kg^{-1} i.p.), both 5-HT$_{1A}$ + 5-HT$_{2A}$ with 8-OH-DPAT/DOI (8-OH-DPAT 1 mg kg^{-1} i.p., DOI 0.5 mg kg^{-1} i.p.) and vehicle control (Fig. 7c and Extended Data Fig. 9a). Across these treatment groups, we did not observe a psilocybin-like (complete) abolishment effect on mechanical hypersensitivity (Fig. 7d). We observed a modest improvement in mechanical allodynia in the 8-OH-DPAT and 8-OH-DPAT + DOI treatment groups on post-treatment day 1 (Fig. 7d and Extended Data Fig. 9b). When these SNI mice treated with 8-OH-DPAT or 8-OH-DPAT + DOI were tested in the EPM and TST there was no statistically significant improvement (Fig. 7e,f and Extended Data Fig. 9c). SNI mice treated with DOI only displayed increased mobility time in TST ($P = 0.028$) without any improvement in mechanical hypersensitivity or EPM (Fig. 7c-f (top)). Thus, taken together, our data indicate that the therapeutic effects of psilocybin on mechanical hypersensitivity and anxiodepressive-like behaviors are mediated by the coactivation of 5-HT$_{2A}$ and 5-HT$_{1A}$ receptors (Figs. 6 and 7g). However, achieving these effects appears to depend on psilocybin's partial agonist activity, as full agonism did not produce similar behavioral responses (Fig. 7e–h).

Discussion

Chronic pain and mood dysfunction are interconnected, often forming a vicious cycle that poses substantial challenges for patients in clinical settings[1]. The presence of pain can complicate the treatment of depression, as poorly managed or treatment-resistant pain is frequently associated with worse depression outcomes[2]. Conversely, depression in patients experiencing pain is linked to increased pain complaints and greater functional impairment. Reflecting this interplay, we observed a strong correlation between mechanical allodynia and anxiodepressive-like behaviors in all tested SNI and CFA mice (Figs. 1 and 2). While intraplantar CFA injections are commonly used to model sub-acute inflammatory pain, we modified established protocols[27,29] by increasing the CFA injection volume beyond conventional limits to induce a chronic mechanical allodynic state (Extended Data Fig. 1b). The resulting CFA phenotype exhibited comparable levels of mechanical hypersensitivity, affective-related behavior changes and impaired motor skill performance to those observed in SNI mice (Extended Data Fig. 1c). We suspect this transformation of an acute inflammatory pain model to a chronic one is likely driven by an overwhelming inflammatory response, persistent immune signaling and/or alterations in peripheral nerve function.

Consistent with emerging observations of psilocybin's therapeutic potential in treating chronic pain[22,23], we found behavioral evidence that a single dose of psilocybin induced a rapid and sustained reversal of chronic neuropathic and inflammatory pain-like states and its associated affective state. Building on recent findings mentioned in ref. 22, which demonstrated that administering psilocybin immediately after a pain-inducing procedure (formalin injection) attenuates the development of a chronic pain-like state, and ref. 23 showing psilocybin can reverse pain-like behaviors in both chemotherapy-induced peripheral neuropathy and CFA rodent models, psilocybin appears to have the potential to both block the onset of chronic pain syndromes through an acute mechanism and reverse established chronic pathology (Fig. 1). In this study, we selected a psilocybin dose of 0.5 mg kg^{-1}, representing the inflection points on the dose–response curve in the HTR assay and open field test (Fig. 1b,c). This dose is half of what was used in the aforementioned rodent studies, allowing us to explore efficacy at a lower threshold. These pain experiments are congruent with other studies; the 0.5 mg kg^{-1} dose is likely to induce neural plasticity, as behavioral improvements (and forms of learning) and neuronal structural remodeling have been observed in this dose range, 0.3–1.0 mg kg^{-1} (refs. 35,36). Future studies in both human and rodent models of chronic pain will be crucial for identifying optimal dosing strategies that elicit behavioral and neurophysiological evidence of neural plasticity.

The concurrent alleviation of both pain models and behaviors associated with affective states indicates the likely convergence of pathological processes within supraspinal regions. Several lines of evidence argue that psilocybin's reversal of SNI- and CFA-induced chronic pain states stem from neocortical mechanisms. We show that (1) SNI/CFA mice developed a strong association (formation and recall of preference) with the psilocybin-paired chamber as compared with saline (Fig. 3), (2) local application of psilocin to the ACC normalizes chronic pain-associated hyperactivity (Fig. 5) and (3) local application of psilocin to bilateral ACC rapidly reverses mechanical allodynia and depression-like behavior (Fig. 4i,j). Thus, it appears that the neurophysiological and behavioral effects of chronic mechanical allodynia and its reversal induced by psilocin are, to a large degree, cortical phenomena. We suspect that psilocin-induced suppression of heightened spontaneous activity in ACC pyramidal neurons may act to rapidly recalibrate hypersensitivity behavior[15]. It has been shown that inhibiting ACC pyramidal neurons[37] or activating inhibitory neurons[38] can acutely reduce hypersensitivity induced by CFA or formalin. Simultaneously, psilocin may engage additional cortical neurons and circuits, both locally and across broader connected networks tied to descending pain modulation[39] through its complex pharmacology and alterations of neuronal excitability[40]. The duration of this acute activity reconfiguration and its potential to facilitate other forms of circuit adaptations, which may underlie the observed sustained improvements—such as dendritic growth and new synapse formation—remain important areas for further investigation.

Psychedelics are widely recognized as 5-HT_{2A} receptor agonists, yet their mechanism of action is far more complex and multifaceted than initially understood[41]. Psilocin is now considered to be relatively nonselective for 5-HT_2 receptors, displaying moderate to high affinity for 5-HT_{1A} and 5-HT_{2A} subtypes[42]. Both 5-HT_{2A} and 5-HT_{1A} receptors are strongly expressed in the PFC[32,43,44] with comparable distribution across excitatory (~50–70%) and inhibitory (~20–30%) cell types[45]. Single-cell analyses of PFC neurons suggest coexpression of 5-HT_{2A} and 5-HT_{1A} receptors[46] implying that serotonin and psychedelics may exert dynamic excitatory (via 5-HT_{2A}) or inhibitory (via 5-HT_{1A}) effects within the same cell depending on their expression ratio and subcellular localization. Selective pharmacological agonism of 5-HT_{2A} and 5-HT_{1A} receptors would drive pyramidal neuronal excitability[47] and hyperpolarization[48], respectively. In our study, pharmacologically blocking either 5-HT_{2A} or 5-HT_{1A} receptors before psilocybin administration completely abolished its rapid and sustained effects on mechanical hypersensitivity and anxiodepressive-like behaviors (Fig. 6). This suggests that altering the balance between 5-HT_{2A} and 5-HT_{1A} receptor activity—whether by favoring 5-HT_{2A} over 5-HT_{1A} (as with WAY-100635) or 5-HT_{1A} over 5-HT_{2A} (as with pimavanserin)—is insufficient to produce therapeutic effects.

Supporting this conclusion, administration of selective full agonists such as DOI (highly selective for 5-HT_2 receptors (A, B, C) with a 1000-fold selectivity over 5-$HT1_A$ receptors[49]) or 8-OH-DPAT (highly selective for 5-HT_{1A} agonist) alone failed to produce psilocin-like effects on either mechanical allodynia or behaviors assessed in the EPM and TST (Fig. 7). Interestingly, combined full agonism with DOI and 8-OH-DPAT failed to replicate psilocybin's effects (Fig. 7). This might suggest that partial agonist activity, as seen with psilocin, is critical for achieving the nuanced modulation of receptor activity required for therapeutic efficacy. Additional studies coupling receptor-specific antagonists to psilocybin or new partial agonists[41] in chronic pain patients will clarify whether acute activation of 5-HT_{2A} or 5-HT_{1A} receptors is necessary for therapeutic effect.

While selective activation of 5-HT_{2A} or 5-HT_{1A} receptors alone failed to replicate psilocybin's effects on mechanical allodynia and anxiodepressive-like behaviors in SNI mice, two-photon calcium imaging with these specific agonists revealed receptor-specific trends on neuronal activity consistent with prior electrophysical recordings[50]. Local application of DOI-induced activation in L2/3 pyramidal neurons, whereas 8-OH-DPAT produced a net suppressive effect (Fig. 7a,b). Interestingly, the combination of DOI and 8-OH-DPAT elicited a psilocin-like response, characterized by an intermediate effect that inhibited spontaneously hyperactive neurons and activated previously silent neurons. We propose that in SNI/CFA, chronic pain-like states, hyperactive circuits emerge in pain-related affective nodes, like in the ACC. This process of chronification may also modify gene expression and/or sensitivity of serotonergic receptors, characterized by increased 5-HT_{2A} and decreased 5-HT_{1A} receptor activity in these regions, thereby contributing to hyperexcitable state (Fig. 7g). Psilocin, acting as a nonselective partial agonist at 5-HT receptors, may (1) rapidly attenuate excessive neuronal firing via 5-HT_{1A} receptor activation, (2) restore neuronal activity in other cell types that support descending pain modulation and enhanced mood processing facilitated by 5-HT_{2A} receptor activation and (3) reestablish balanced 5-HT_{2A} and 5-HT_{1A} receptor expression and signaling within individual neurons (Fig. 7h). Some of these effects could be due to psilocin's signaling at other 5-HT receptors including 2B, 2C and even directly at TrkB. Nevertheless, this interplay between receptor subtypes underscores the unique mechanisms by which psilocybin exerts its therapeutic effects in chronic pain-like states with comorbid mood dysfunction.

Online content

Any methods, additional references, Nature Portfolio reporting summaries, source data, extended data, supplementary information, acknowledgements, peer review information; details of author contributions and competing interests; and statements of data and code availability are available at https://doi.org/10.1038/s41593-025-02068-0.

References

1. De La Rosa, J. S. et al. Co-occurrence of chronic pain and anxiety/depression symptoms in U.S. adults: prevalence, functional impacts, and opportunities. *Pain* **165**, 666–673 (2024).
2. Bair, M. J., Robinson, R. L., Katon, W. & Kroenke, K. Depression and pain comorbidity: a literature review. *Arch. Intern. Med.* **163**, 2433–2445 (2003).
3. Michaelides, A. & Zis, P. Depression, anxiety and acute pain: links and management challenges. *Postgrad. Med.* **131**, 438–444 (2019).
4. Brooks, J. M. et al. Pain intensity, depressive symptoms, and functional limitations among older adults with serious mental illness. *Aging Ment. Health* **23**, 470–474 (2019).
5. Sheng, J., Liu, S., Wang, Y., Cui, R. & Zhang, X. The link between depression and chronic pain: neural mechanisms in the brain. *Neural Plast.* **2017**, 9724371 (2017).
6. Talbot, J. D. et al. Multiple representations of pain in human cerebral cortex. *Science* **251**, 1355–1358 (1991).
7. Barthas, F. et al. The anterior cingulate cortex is a critical hub for pain-induced depression. *Biol. Psychiatry* **77**, 236–245 (2015).
8. Zhou, W. et al. A neural circuit for comorbid depressive symptoms in chronic pain. *Nat. Neurosci.* **22**, 1649–1658 (2019).
9. Zhao, R. et al. Neuropathic pain causes pyramidal neuronal hyperactivity in the anterior cingulate cortex. *Front. Cell. Neurosci.* **12**, 107 (2018).
10. Bliss, T. V. P., Collingridge, G. L., Kaang, B.-K. & Zhuo, M. Synaptic plasticity in the anterior cingulate cortex in acute and chronic pain. *Nat. Rev. Neurosci.* **17**, 485–496 (2016).
11. Naylor, B. et al. Reduced glutamate in the medial prefrontal cortex is associated with emotional and cognitive dysregulation in people with chronic pain. *Front. Neurol.* **10**, 460034 (2019).
12. Blom, S. M., Pfister, J.-P., Santello, M., Senn, W. & Nevian, T. Nerve injury-induced neuropathic pain causes disinhibition of the anterior cingulate cortex. *J. Neurosci.* **34**, 5754–5764 (2014).
13. Foltz, E. L. & White, L. E. Jr. Pain 'relief' by frontal cingulumotomy. *J. Neurosurg.* **19**, 89–100 (1962).
14. Zhang, Q. et al. Chronic pain induces generalized enhancement of aversion. *eLife* **6**, e25302 (2017).
15. Sellmeijer, J. et al. Hyperactivity of anterior cingulate cortex areas 24a/24b drives chronic pain-induced anxiodepressive-like consequences. *J. Neurosci.* **38**, 3102–3115 (2018).
16. George, M. S., Ketter, T. A. & Post, R. M. Prefrontal cortex dysfunction in clinical depression. *Depression* **2**, 59–72 (1994).
17. Nestler, E. J. et al. Neurobiology of depression. *Neuron* **34**, 13–25 (2002).
18. Zheng, C. J., Van Drunen, S. & Egorova-Brumley, N. Neural correlates of co-occurring pain and depression: an activation-likelihood estimation (ALE) meta-analysis and systematic review. *Transl. Psychiatry* **12**, 196 (2022).
19. Nichols, D. E. Psilocybin: from ancient magic to modern medicine. *J. Antibiot.* **73**, 679–686 (2020).
20. Halberstadt, A. L. & Geyer, M. A. Multiple receptors contribute to the behavioral effects of indoleamine hallucinogens. *Neuropharmacology* **61**, 364–381 (2011).
21. Lyes, M., Yang, K. H., Castellanos, J. & Furnish, T. Microdosing psilocybin for chronic pain: a case series. *Pain* **164**, 698–702 (2023).
22. Kolbman, N. et al. Intravenous psilocybin attenuates mechanical hypersensitivity in a rat model of chronic pain. *Curr. Biol.* **33**, R1282–R1283 (2023).
23. Koseli, E. et al. IUPHAR Article: psilocybin induces long-lasting effects via 5-HT2A receptors in mouse models of chronic pain. *Pharmacol. Res.* **215**, 107699 (2025).
24. Ross, S. Therapeutic use of classic psychedelics to treat cancer-related psychiatric distress. *Int Rev. Psychiatry* **30**, 317–330 (2018).
25. Kuromaru, S., Okada, S., Hanada, M., Kasahara, Y. & Sakamoto, K. The effect of LSD on the phantom limb phenomenon. *J. Lancet* **87**, 22–27 (1967).
26. Raison, C. L. et al. Single-dose psilocybin treatment for major depressive disorder: a randomized clinical trial. *JAMA* **330**, 843–853 (2023).
27. Larson, A. A., Brown, D. R., el-Atrash, S. & Walser, M. M. Pain threshold changes in adjuvant-induced inflammation: a possible model of chronic pain in the mouse. *Pharmacol. Biochem. Behav.* **24**, 49–53 (1986).
28. Decosterd, I. & Woolf, C. J. Spared nerve injury: an animal model of persistent peripheral neuropathic pain. *Pain* **87**, 149–158 (2000).
29. Liu, X. J. et al. Treatment of inflammatory and neuropathic pain by uncoupling Src from the NMDA receptor complex. *Nat. Med.* **14**, 1325–1332 (2008).
30. Marlier, L., Teilhac, J. R., Cerruti, C. & Privat, A. Autoradiographic mapping of 5-HT1, 5-HT1A, 5-HT1B and 5-HT2 receptors in the rat spinal cord. *Brain Res.* **550**, 15–23 (1991).
31. Doly, S. et al. The 5-HT2A receptor is widely distributed in the rat spinal cord and mainly localized at the plasma membrane of postsynaptic neurons. *J. Comp. Neurol.* **472**, 496–511 (2004).
32. Chiu, Y.-T. et al. A suite of engineered mice for interrogating psychedelic drug actions. Preprint at *bioRxiv* https://doi.org/10.1101/2023.09.25.559347 (2023).
33. Meltzer, H. Y. et al. Pimavanserin, a serotonin(2A) receptor inverse agonist, for the treatment of Parkinson's disease psychosis. *Neuropsychopharmacology* **35**, 881–892 (2010).
34. Fletcher, A. et al. Electrophysiological, biochemical, neurohormonal and behavioural studies with WAY-100635, a potent, selective and silent 5-HT1A receptor antagonist. *Behav. Brain Res.* **73**, 337–353 (1995).
35. Nardou, R. et al. Psychedelics reopen the social reward learning critical period. *Nature* **618**, 790–798 (2023).
36. Shao, L.-X. et al. Psilocybin induces rapid and persistent growth of dendritic spines in frontal cortex in vivo. *Neuron* **109**, 2535–2544 (2021).
37. Kang, S. J. et al. Bidirectional modulation of hyperalgesia via the specific control of excitatory and inhibitory neuronal activity in the ACC. *Mol. Brain* **8**, 81 (2015).
38. Gu, L. et al. Pain inhibition by optogenetic activation of specific anterior cingulate cortical neurons. *PLoS ONE* **10**, e0117746 (2015).
39. Zhang, L., Zhang, Y. & Zhao, Z.-Q. Anterior cingulate cortex contributes to the descending facilitatory modulation of pain via dorsal reticular nucleus. *Eur. J. Neurosci.* **22**, 1141–1148 (2005).
40. Andrade, R. Serotonergic regulation of neuronal excitability in the prefrontal cortex. *Neuropharmacology* **61**, 382–386 (2011).
41. Wallach, J., et al. Identification of 5-HT receptor signaling pathways associated with psychedelic potential. *Nat. Commun.* **14**, 8221 (2023).
42. Erkizia-Santamaría, I. et al. Serotonin 5-HT2A, 5-HT2c and 5-HT1A receptor involvement in the acute effects of psilocybin in mice. In vitro pharmacological profile and modulation of thermoregulation and head-twich response. *Biomed. Pharmacother.* **154,** 113612 (2022).
43. Goodfellow, N. M., Benekareddy, M., Vaidya, V. A. & Lambe, E. K. Layer II/III of the prefrontal cortex: inhibition by the serotonin 5-HT1A receptor in development and stress. *J. Neurosci.* **29**, 10094–10103 (2009).
44. del Olmo, E. et al. Early localization of mRNA coding for 5-HT1A receptors in human brain during development. *Brain Res. Mol. Brain Res.* **60**, 123–126 (1998).

45. Santana, N., Bortolozzi, A., Serrats, J., Mengod, G. & Artigas, F. Expression of serotonin1A and serotonin2A receptors in pyramidal and GABAergic neurons of the rat prefrontal cortex. *Cereb. Cortex* **14**, 1100–1109 (2004).
46. Savalia, N. K., Shao, L.-X. & Kwan, A. C. A dendrite-focused framework for understanding the actions of ketamine and psychedelics. *Trends Neurosci.* **44**, 260–275 (2021).
47. Tang, Z.-H. et al. The effects of serotonergic psychedelics in synaptic and intrinsic properties of neurons in layer II/III of the orbitofrontal cortex. *Psychopharmacol.* **240**, 1275–1285 (2023).
48. Riad, M. et al. Somatodendritic localization of 5-HT1A and preterminal axonal localization of 5-HT1B serotonin receptors in adult rat brain. *J. Comp. Neurol.* **417**, 181–194 (2000).
49. Pierce, P. A. & Peroutka, S. J. Hallucinogenic drug interactions with neurotransmitter receptor binding sites in human cortex. *Psychopharmacol.* **97**, 118–122 (1989).
50. Araneda, R. & Andrade, R. 5-Hydroxytryptamine2 and 5-hydroxytryptamine 1A receptors mediate opposing responses on membrane excitability in rat association cortex. *Neuroscience* **40**, 399–412 (1991).

Methods

Experimental animals

All mice were maintained at the University of Pennsylvania, Perelman School of Medicine, John Morgan animal facility with normal dark/light cycle, controlled room temperature and humidity conditions and had free access to food and water. All animal handling was under guidelines set forth by the School of Medicine's Institutional Animal Care and Use Committee, approved protocol 807237. C57/BL6 males at an age range of 8–12 weeks were used for behavioral experiments. SNI/CFA and sham controls were housed in cages with five in each cage, with ample food and water. Animals were assigned to groups randomly and no animals were excluded from analysis.

Modeling chronic pain and von Frey testing

SNI of the sciatic nerve or sham operation (sham) was performed on C57BL/6 adult mice (8–12 weeks)[51] In brief, surgeries were performed under strict sterile conditions. Mice were deeply anesthetized, and a small incision in the left thigh was made to expose the sciatic nerve. The tibial and common peroneal nerves were then axotomized/ligated, leaving the sural nerve intact. Care was taken to avoid any contact with or stretching of the intact sural nerve. Muscle and skin were closed in two layers. For sham surgery, the sciatic nerve was exposed but not ligated or cut. For inducing a model of inflammatory pain, undiluted CFA (Sigma-Aldrich, F5881) was subcutaneously injected unilaterally into the intraplantar surface of one hind paw in the mice (~80–100 µl), whereas control mice were injected with 0.9% saline solution (~80 µl). The von Frey test was used to assess the onset and maintenance of mechanical allodynia over time. In all animal groups, mechanical threshold was examined using an Electronic von Frey anesthesiometer (IITC, Life Science Instruments) that measures the precise minimum pressure at which paw withdrawal occurs. Specifically, a von Frey tip of suitable rigidity was attached to an electronic probe and used to apply an increasing pressure to the lateral plantar aspect (the sural nerve skin territory) of the hind paw. The anesthesiometer displays the pressure at which the mouse retracts from the von Frey tip. Three trials for paw withdrawal were recorded for each day tested and an average was reported. The von Frey test was performed during the light cycle by the same researcher.

Behavioral tests

HTR assessment. HTR is described as a rotational/side-to-side head movement that spontaneously occurs following psychedelic administration[41]. HTR was assessed in individual animals in an Open Field chamber (25 × 25cm) for 30 min immediately after psilocybin injection. A 30-min session was recorded with a video camera and subsequently scored offline by a trained observer.

EPM. EPM consisted of two open arms without walls and two closed arms with walls. Time spent within open and closed arms was measured using ANY-maze software for a period of 5 min. Mice were placed in the center of an elevated maze, facing an open arm, to start the test. The maze is cleaned with ethanol and dried with paper towels before each test.

FST. A cylindrical glass tank (30 cm height × 20 cm diameter) was filled with water (maintained at 23–25 °C) to a height of 15 cm. Each tank is separated from an adjacent tank using a divider. Animals were lowered gently into water by tail and allowed to swim for 6 min. Only the last 4 min of the test were analyzed for periods of mobility, which were considered to be any movements other than those required to tread water.

OFT. The test was conducted in a 50 × 50 cm arena with a 25 × 25 cm central zone marked in the center. Before each experiment, the chamber was cleaned with 70% ethanol and allowed to dry completely. At the start of the trial, the animal was gently placed in the center of the arena, and behavioral recording using the ANY-maze system was initiated. During the 5-min session, the following parameters were measured: the number of entries into the central zone, the total distance traveled and the time spent in the central zone.

Light/dark box test. The test was conducted in a 45 × 30 × 27 cm box, divided into two compartments—one-third was a covered, dark chamber and the remaining two-thirds was an open, light chamber. The compartments were connected by a 7.5 × 7.5 cm opening, allowing the mouse to move freely between them. White lights were illuminated above the light chamber during the test. The time spent in the light and dark chambers was recorded using ANY-maze software over 10 min. At the start of the trial, the mouse was gently placed in the opening between the compartments, facing the dark chamber. Before each test, the arena was cleaned with 70% ethanol and thoroughly dried with paper towels.

TST. A hollow plastic cylinder is placed around the base of the mouse's tail to prevent tail climbing. The mouse is then suspended by its tail using a long piece (~15 cm) of strong adhesive tape to the top of the testing system. The test lasts for 6 min but only the final 4 min of the test were analyzed for periods of mobility using ANY-maze software.

Rotarod test. Using the AccurRotor EzRod system, set up rotarod to accelerate from 1 to 45 rpm over 80 s for a total period of 180 s. Gently place the mouse on the rod and start the experiment. The trial begins with the start of the rotation and ends when a mouse falls off the rod. If a mouse clings to the rod and completes a full rotation (while hanging on to the rod), the time for the mouse is stopped and counts as a fall. The test is repeated for three trials and the average of the trials is used. If the mouse falls within the first 10 s of the test, the test is repeated. The latency to fall is then analyzed. Rod is cleaned with 70% ethanol and dried with delicate task wipes before each trial.

CPP. CPP apparatus consists of two chambers with distinct visual cues. One chamber with rectangular-shaped cues and another with circular cues on the walls of the chamber. The chambers are connected by a neutral third chamber with partitions on either side. During the preconditioning phase, the partitions were removed and the mouse was gently placed in the neutral chamber, allowing it to explore the different areas. Immediately after, time spent in each chamber over 15 min was recorded using ANY-maze software. The time spent in each chamber is then analyzed to verify that there is no preconditioning preference. Animals spending more than 80% or less than 20% of total time in one chamber are eliminated from the study. On the conditioning day, mice receive vehicle treatment (saline) and are then immediately placed in the appropriate pairing chamber for 30 min with no access to other chambers (using the partitions to block access). The mouse is then removed from the chamber. Four hours after vehicle treatment injection, the mouse is injected with psilocybin and immediately (within 2 min) is gently placed in the opposite pairing chamber for 30 min. Chamber pairings are counterbalanced (one mouse receives psilocybin in the rectangular chamber while another receives it in the circular chamber) to verify that no bias exists towards cues. On the test day (one day following the conditioning day), the mouse is gently placed in the neutral chamber. The partitions are removed such that the mouse has access to all chambers. Immediately after, time spent in each chamber over 15 min was recorded using ANY-maze software. Increased time spent in the psilocybin-paired chamber indicates a preference for the treatment.

Systemic and local drug delivery

In Fig. 1b,c, mouse head-twitch dose–response curves were recorded following intraperitoneal injection of psilocybin (Usona Institute) at doses of 0 mg kg^{-1} (saline), 0.25 mg kg^{-1}, 0.50 mg kg^{-1} and 1.00 mg kg^{-1}.

In Fig. 1d–g, following the development of chronic pain, mice were treated with psilocybin on day 27 via a single i.p. (0.5 mg kg^{-1}) or saline (same volume). In Fig. 6, SNI mice received either pimavanserin (Selleck Chemicals, S8183; 1 mg kg^{-1} i.p. dose) or WAY-100635 (Selleck Chemicals, S2663; 1 mg kg^{-1} i.p. dose) 30 min before psilocybin (0.5 mg kg^{-1}). In Fig. 7b–m, SNI mice received either 8-OH-DPAT (Selleck Chemicals, S8447; 1 mg kg^{-1} i.p. dose), DOI (Cayman Chemical, 13885; 1 mg kg^{-1} i.p. dose) or DOI/DPAT (co-injected with DOI and DPAT; both 1 mg kg^{-1} i.p. dose).

For behavior experiments in Fig. 4, local psilocin injection (Cayman Chemical, 9003135; 1–500 µM mixed with Rhodamine 6G) to either ACC or spinal cord required a brief period of general anesthesia induced by isoflurane (4–5% for induction, 1–2% for maintenance). To ensure proper anesthetic depth, animal reactivity was assessed periodically by gently pinching the hind paws. For bilateral ACC injection, hair over the scalp was shaved, cleaned thrice with ethanol and a midline scalp incision was made using microsurgical tools. We next removed the soft tissue attached to the skull over ACC regions with fine forceps and a microblade. The mouse skull was immobilized by gluing (cyanoacrylate glue) it to a thin metal plate. Once the glue solidified (2 min), a high-speed microdrill was used to thin a small circular area (~ 0.5 mm in diameter) over the ACC bilaterally (+0.5–1.0 mm anterior to the bregma and 0.3–0.5 mm lateral to midline). Intermittent drilling and artificial cerebrospinal fluid (aCSF) immersion minimized heat-induced damage. After the bone thins to ~10–20 µm in thickness, a small bone tear was created with a beveled needle (27G) tip. At this point, a glass electrode filled with psilocin in aCSF (total volume of ~2 µl) was slowly injected into the cortex (depth 200–300 µm) via pressure application with a picospritzer (20 p.s.i., 50 ms per pulse, 1 Hz, 5–10 pulses). Upon completion of injection (~10–15 min), the electrode was rested for ~5–10 min followed by a slow retraction with burr hole closure via a small amount of cyanoacrylate glue. The procedure was repeated for the other hemisphere. The metal plate was then removed, scalp skin reapproximated and sutured.

For the intrathecal psilocin injections, hair overlaying the lower spine was shaved (3 × 3 cm area near base of tail) and cleaned thrice by ethanol. A 15-ml conical tube was placed under the abdomen of the mouse to expose a bigger area of the interspinous ligament, which was punctured by the needle to access the intradural space. Positioning the mouse on a 15-ml conical tube also made it easier to locate and grasp the iliac crest, which is identified by finding the two pits formed at the interface between the muscle and the hip bone. The injection site (L5–L6) was determined by identifying the most protruding spinal process (L6). Of note, injection at this level reduces concern for spinal injury as the spinal cord ends above this level. Next, the animal was grasped just above the hips and a psilocin-loaded Hamilton syringe (1–500 µM, total volume of ~5 µl mixed with Rhodamine 6G) was inserted between the groove of L5 and L6 at a 30° angle and to a depth of 0.5 cm. Once the needle successfully enters the intradural space, the mouse's tail should move or flick. After observation of tail flick (confirmation of correct space), psilocin was slowly injected, and once completed, the syringe was left in place for 10 s to prevent backflow. The syringe was removed, and the animal was returned to its cage for monitoring.

Spinal cord collection and cFos immunohistochemistry

After perfusion, the entire mouse spinal column, including bone and muscles, was extracted by cutting along the length of the animal from the head to the tail. Small portions of the ribs were retained to help identify the thoracic region. The spinal column was cleaned by removing excess muscle from the spinal column using small scissors. Once cleaned to reveal the bone, the spinal column was placed in a dish with PBS under a magnifying lens. Using blunt tweezers to hold the cord, a blade was used to scrape off the remaining muscle until vertebrae and discs were visible. The lumbosacral region was identified (by counting vertebrae from the ribs - the reference for the thoracic region) and isolated. The spinal cord was extracted by using blunt tweezers to hold one end and pointed tweezers to carefully break the discs on the other end.

Lumbosacral spinal cord samples for subsequent cFos immunostaining were embedded in a 7% agar gel and sectioned in 1× PBS on a vibratome (Leica VT1000S) to obtain 30-µm-thick coronal sections. Intact sections were first blocked for 1 h at room temperature in blocking buffer (5% normal goat serum, 0.1% Triton X-100 in 1× PBS), followed by overnight incubation (~16 h) in primary cFos antibody solution (EnCor Biotechnology, RPCA-c-FOS; 1:1,000 rabbit polyclonal) at room temperature. Sections were washed 3× for 10 min each in 1× PBS before a 2 h room temperature incubation in secondary Alexa-Fluor 568 goat anti-rabbit antibody solution (Invitrogen by ThermoFisher Scientific, A-11011; 1:300). A final wash (3× for 10 min each in 1× PBS) was performed before slide mounting with DAPI Fluoromount-G (Southern Biotech, 0100-20).

Fixed sections were imaged on a fluorescence microscope (Keyence BZ-X810) at ×4 (Plan Apochromat, NA = 0.2) using a red cube filter (ex, 545/25 nm; em, 605/70 nm) or by confocal microscope (Thor Cerna confocal system) at ×10 (Plan Fluor, NA = 0.3) using a fixed wavelength 561 nm laser (Coherent OBIS). Confocal images were stitched using Fiji's Grid/collection stitching plug-in[52]. Laminae I and II of the dorsal horn of the spinal cord were manually identified in each section using Fiji (version 2.9.0), and cFos-positive cells were identified in Fiji using a particle analyzer pipeline. Briefly, within each lamina I–II dorsal horn region of interest (ROI), the ROI was manually thresholded, converted to a mask, and then processed with a watershed algorithm to aid in the detection of individual cells. Binarized images were then processed with Fiji's particle detector with size parameters 2–13 $pixels^2$ to calculate the number of cFos-positive cells within each ROI. Each plotted sample in Fig. 4d represents the average cell count from 3–6 ROIs in one animal.

Two-photon calcium imaging in awake animals

The genetically encoded calcium indicator GCaMP6f was used for calcium imaging of pyramidal neurons and interneurons in the cortex. GCaMP6f expression was performed using intracranial AAV injections in neonates. Pyramidal neurons were labeled using recombinant AAV9-*CaMKII*-Cre (Addgene, 105558; 10 nl of AAV per mouse) and AAV9-*CAG*-FLEX-GCaMP6f (Addgene, 100835; 100 nl of AAV per mouse). A glass micropipette (Drummond, 50,001,001 × 10) was pulled and beveled. A plunger was lightly oiled and inserted into the micropipette to pull the AAV mix. Subsequently, pups at postnatal days 1–2 were anesthetized by hypothermia (typically ~ 2–3 min on ice) and the micropipette was used (freehand) to penetrate the skin and skull and deliver ~200 nl of the virus mix. Medial PFC injection site was determined using landmarks—skull suture lines and head veins—as reference points. Imaging was performed in 1–2-month-old mice, using both sexes, after at least 4 weeks of AAV expression. Mice were group-housed in temperature and humidity-controlled rooms on a 12-h light/12-h dark cycle after injections.

In preparation for imaging, mice underwent a surgical procedure to attach a head holder mount and create an imaging window for two-photon microscopy. In brief, mice were anesthetized with a mixture of 100% oxygen at 2 l min^{-1} and 1–4% isoflurane. A heating pad was used to maintain the animal's body temperature at approximately 37 °C. The mouse's head was shaved, and its skull surface was exposed with a midline scalp incision. The periosteal tissue over the skull surface was removed without damaging the temporal and occipital muscles. A head holder consisting of two parallel metal bars was attached to the animal's skull. In Cre-positive mice injected with AAV, <1% of mice were negative for GCaMP, suggesting off-target injection was a rare event. In positive mice, a small skull region (~2–4mm in diameter) located over the interfrontal suture was removed, and a round glass coverslip (approximately the same size as the bone being removed) was affixed to

the skull with Loctite 495, followed by dental acrylic cement. This window enabled imaging of ACC (+0.5–1.0 mm anterior to the bregma and 0.1–0.3 mm lateral to midline). On recovering from surgical anesthesia, mice with head mounts were habituated daily (two sessions of 30 min with 15-min break) starting on postoperative day 1 in a custom-built body support to minimize potential stress effects of head restraining and imaging. No obvious distress was observed in habituated animals during imaging experiments. Mice tolerated surgery and stress related to the perioperative period as indicated by a 0–10% drop in weight. Imaging experiments were started on postoperative days 2–3 after window implantation.

On the day of imaging, awake mice were positioned in the custom head holder device under the two-photon microscope. In vivo two-photon imaging was performed with an Olympus DIY RS two-photon system (tuned to 910–920 nm) equipped with a Coherent Discovery NX laser. We minimized movement-associated image artifacts by head (secured metal head bars) and body (with a plastic sleeve) restraint on the imaging platform. Mice were head-restrained and imaged for <1 h in total, imaging across several regions in L2/3. To avoid potential interference from psilocin-induced activity-dependent plasticity, animals received a single local dose of psilocin via a small bone flap lateral to the cranial window, which was large enough to accommodate the tip of a glass electrode loaded with Rhodamine 6G and psilocin. Pyramidal neurons in ACC region were randomly chosen and recorded for 2-min sessions under awake conditions and once again after local application of psilocin. All experiments were performed using a ×20 Olympus objective (XLUMPLFLN; NA = 1.00, 2.0 mm working distance) immersed in aCSF, with ×2 digital zoom. Images were acquired at a frame rate of 2–4 Hz (2-µs pixel dwell time). Image acquisition was performed using Olympus Fluoview software and analyzed post hoc using ImageJ software version 2.1.0.

During recordings, motion-related artifacts were typically less than 2 µm. Vertical movements were infrequent and minimized by two metal bars attached to the animal's skull (described above) and a custom-built body support. All time-lapse images from each field of view were motion-corrected and referenced to a single template frame using cross-correlation image alignment (TurboReg plugin for ImageJ version 2.1.0). ROIs corresponding to visually identifiable somas (pyramidal cells) were selected manually from the field of view. Imaging planes were acquired from L2/3 corresponding to cells positioned ~150–350 µm from the pial surface, respectively. Note that our neonatal injections produced sparse to moderate labeling of GCaMP6. As shown in Fig. 5, 5–20 neurons per L2/3 imaging region were common. A typical experiment would include 3–4 (randomly chosen) imaging regions per animal, yielding ~20–40 cells per animal. Somas that could be identified in all imaging sessions were included in the dataset.

In this study, we used GCaMP6f, an indirect reporter of neuronal spiking activity. All the pixels inside the ROI were averaged to obtain a fluorescence trace for each ROI. Background fluorescence was calculated as the average pixel value per frame from a region without GCaMP expression (blood vessel) and subtracted from the time-series fluorescence traces. The baseline (F_0) of the fluorescence trace was estimated as the average of inactive portions of the traces (~2 s). We did not smooth the raw fluorescence trace (raw traces are presented throughout the paper in each figure). The $\Delta F/F_0$ (%) was calculated as $\Delta F/F_0 = (F - F_0)/F_0 \times 100$. GCaMP6f can produce large fluorescence transients (20% $\Delta F/F$) in response to single action potentials, and individual spikes within a burst result in stepwise increases in fluorescence. However, when neuronal firing rates are high, it becomes difficult to resolve the number of action potentials owing to the long decay time constant of GCaMP6 fluorescence. We found that there was a diversity in calcium traces of pyramidal cells, which likely reflects burst and non-burst firing. To compare neuronal activity among different cells with activity patterns, we performed an integrated measurement of a cell's output activity over 2 min recording, termed area under the curve (%), as well as measuring peak fluorescence signal. In Figs. 4h and 7b, we report calcium activity changes following drug administration as response ratio, calculated as $\text{response}_{\text{drug}}/\text{response}_{\text{baseline}}$. To express the relative change from baseline, we computed the response ratio of −1, where positive values indicate an increase in activity relative to baseline and negative values indicate a decrease.

Statistics

Summary data were presented as mean ± s.e.m. Power analysis was used to determine sample sizes for Figs. 1 and 2, while sample sizes among other figures are similar to those reported in our previous publications[53–55] and others[9,56,57]. Data distribution was assumed to be normal, but this was not formally tested. The interventions were not blinded, as nearly all experiments were carried out and analyzed by A.H. However, J.C., who was blinded to all experimental groups, conducted independent analyses on all datasets. Detailed statistical methods are included in Supplementary Table 1. Exact P values and common levels of significance (not significant, $P > 0.05$; $^{*}P < 0.05$; $^{**}P < 0.01$; $^{***}P < 0.001$) are reported in Figs. 1–7 and Supplementary Table 1. All statistical analyses were performed using GraphPad Prism.

Reporting summary

Further information on research design is available in the Nature Portfolio Reporting Summary linked to this article.

Data availability

All data needed to evaluate the conclusions and replicate the figures presented in this article are provided in the source data and associated data will be available to the scientific community via figshare at https://figshare.com/s/aae99484130e22266bbc (ref. 58). Source data are provided with this paper.

Code availability

No new code was used in processing of data presented.

References

51. Cichon, J., Sun, L. & Yang, G. Spared nerve injury model of neuropathic pain in mice. *Bio. Protoc.* **8**, e2777 (2018).
52. Preibisch, S., Saalfeld, S. & Tomancak, P. Globally optimal stitching of tiled 3D microscopic image acquisitions. *Bioinformatics* **25**, 1463–1465 (2009).
53. Cichon, J. et al. Ketamine triggers a switch in excitatory neuronal activity across neocortex. *Nat. Neurosci.* **26**, 39–52 (2023).
54. Cichon, J., Blanck, T. J. J., Gan, W.-B. & Yang, G. Activation of cortical somatostatin interneurons prevents the development of neuropathic pain. *Nat. Neurosci.* **20**, 1122–1132 (2017).
55. Cichon, J. et al. Nitrous oxide activates layer 5 prefrontal neurons via SK2 channel inhibition for antidepressant effect. *Nat. Commun.* **16**, 2999 (2025).
56. Adler, A., Zhao, R., Shin, M. E., Yasuda, R. & Gan, W.-B. Somatostatin-expressing interneurons enable and maintain learning-dependent sequential activation of pyramidal neurons. *Neuron* **102**, 202–216 (2019).
57. Yang, G. et al. Sleep promotes branch-specific formation of dendritic spines after learning. *Science* **344**, 1173–1178 (2014).
58. Hammo_SourceData_All.xlsx. *figshare* https://figshare.com/s/aae99484130e22266bbc?file=57293450 (2025).

Acknowledgements

We thank M. Fina for help with animal breeding and management and A. Proekt for helpful discussions and feedback. This work was supported by the National Institutes of Health (R35GM151160-01) and the ASRA Chronic Pain Medicine Research (awarded to J.C.).

Author contributions

J.C. and A.H. initiated the project and wrote the paper with input from all authors. A.H. acquired, processed and analyzed the behavioral data. J.C. performed the calcium imaging in ACC and spinal cord injections. S.W. collected and analyzed the cFos data.

Competing interests

The authors declare no competing interests.

Additional information

Extended data is available for this paper at https://doi.org/10.1038/s41593-025-02068-0.

Supplementary information The online version contains supplementary material available at https://doi.org/10.1038/s41593-025-02068-0.

Correspondence and requests for materials should be addressed to Joseph Cichon.

Peer review information *Nature Neuroscience* thanks Rohini Kuner and the other, anonymous, reviewer(s) for their contribution to the peer review of this work.

https://doi.org/10.1038/s41593-025-02068-0

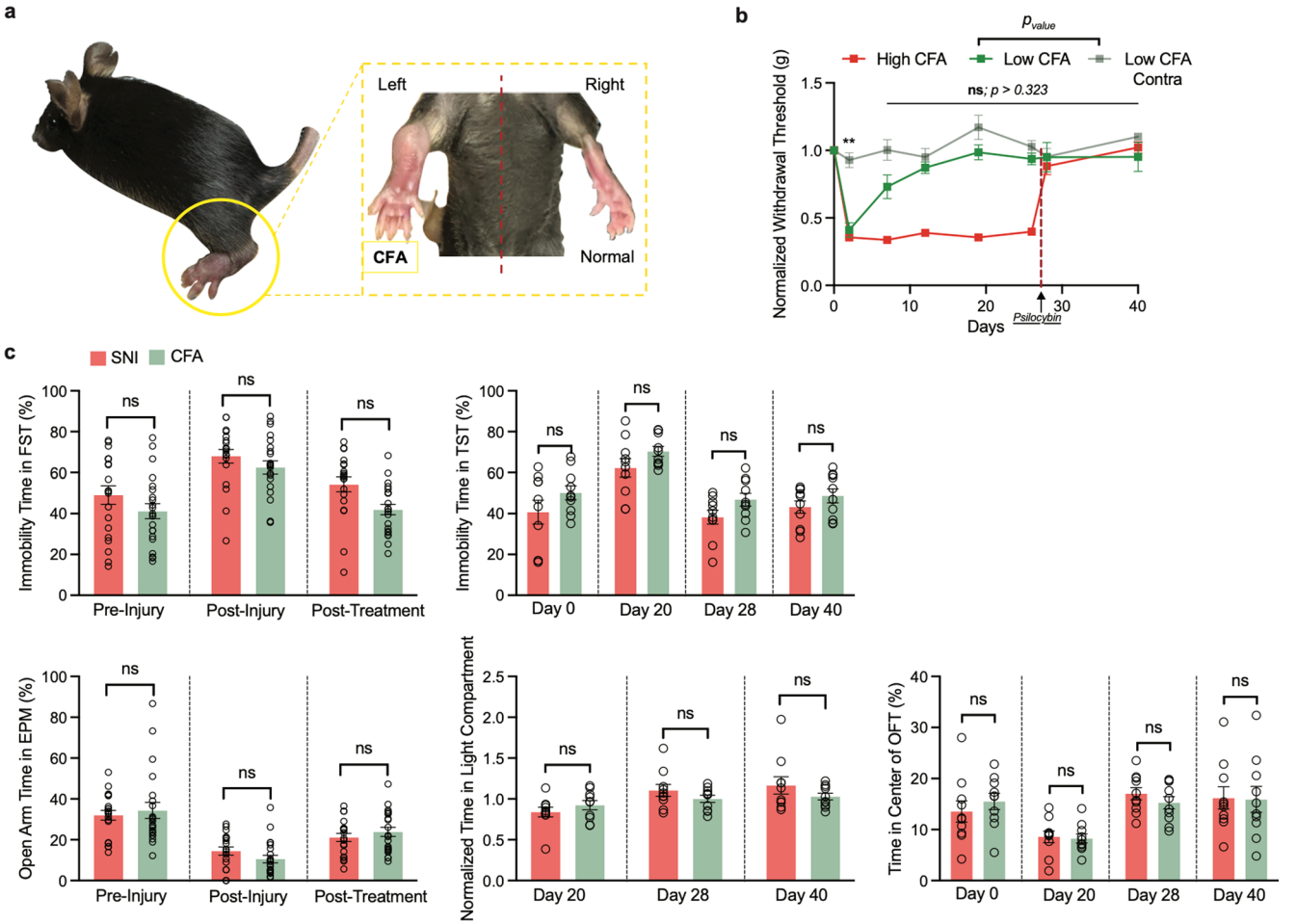

Extended Data Fig. 1 | High volume CFA injection into the hindlimb footpad induces persistent mechanical allodynia. a, Representative photograph of a mouse injected with high volume of CFA in the left hind paw (circled in yellow), showing visible fullness and swelling compared to the contralateral hindlimb footpad at day 20 post-injection. The inset highlights the difference between the CFA-injected (left) and the contralateral hindlimb footpad (right). Data are represented as mean ± s.e.m. **b**, Normalized mechanical withdrawal thresholds for high (*n = 22)* (red) and low (green) (*n = 5)* CFA volume animals over the experimental timeline. High CFA animals display a persistent reduction in withdrawal thresholds as compared to the low volume CFA animals. Low CFA animals display a transient mechanical hypersensitivity with thresholds returning to baseline by day 7 post-CFA injection compared to the contralateral limb (two-way ANOVA, *P > 0.322* after day 7). **c**, Comparison of multiple mood-related behavioral responses (top: FST, TST; bottom: EPM, light/dark test, and OFT) between SNI (*n* = 20) and high-volume CFA (*n* = 22) mice. CFA mice display similar behavior to SNI mice across all mood-related tests (Kruskal–Wallis followed by Dunn's multiple comparison: P > 0.10). Data are represented as mean ± s.e.m. ***P* < 0.01, ns = nonsignificant. Detailed statistics are reported in Supplementary Table 1h.

https://doi.org/10.1038/s41593-025-02068-0

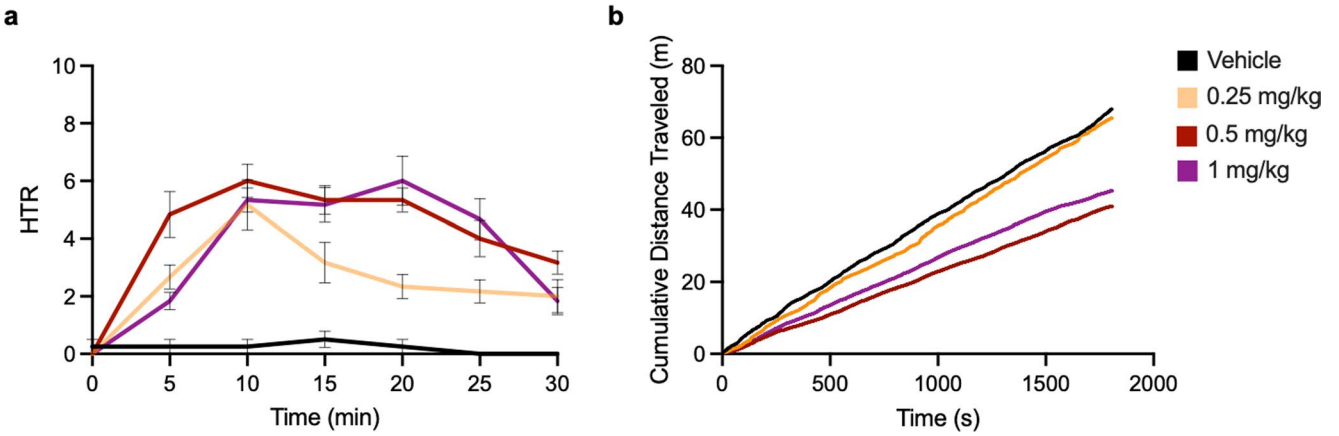

Extended Data Fig. 2 | Different doses of psilocybin elicit distinct behavioral responses following injection. a, Intraperitoneal injection of psilocybin induces a transient head twitch response (HTR) over a dosing range of 0.25 mg/kg ($n = 6$), 0.5 mg/kg ($n = 6$), and 1 mg/kg ($n = 6$). Head twitches are summed every 5 min over the first 30 min post-injection. **b**, Cumulative distance traveled in the open field in animals receiving different psilocybin doses. Higher doses of psilocybin (both 0.5 mg/kg and 1 mg/kg) elicit a hypoactivity state as compared to vehicle controls and psilocybin at 0.25 mg/kg. Data are represented as mean ± s.e.m.

https://doi.org/10.1038/s41593-025-02068-0

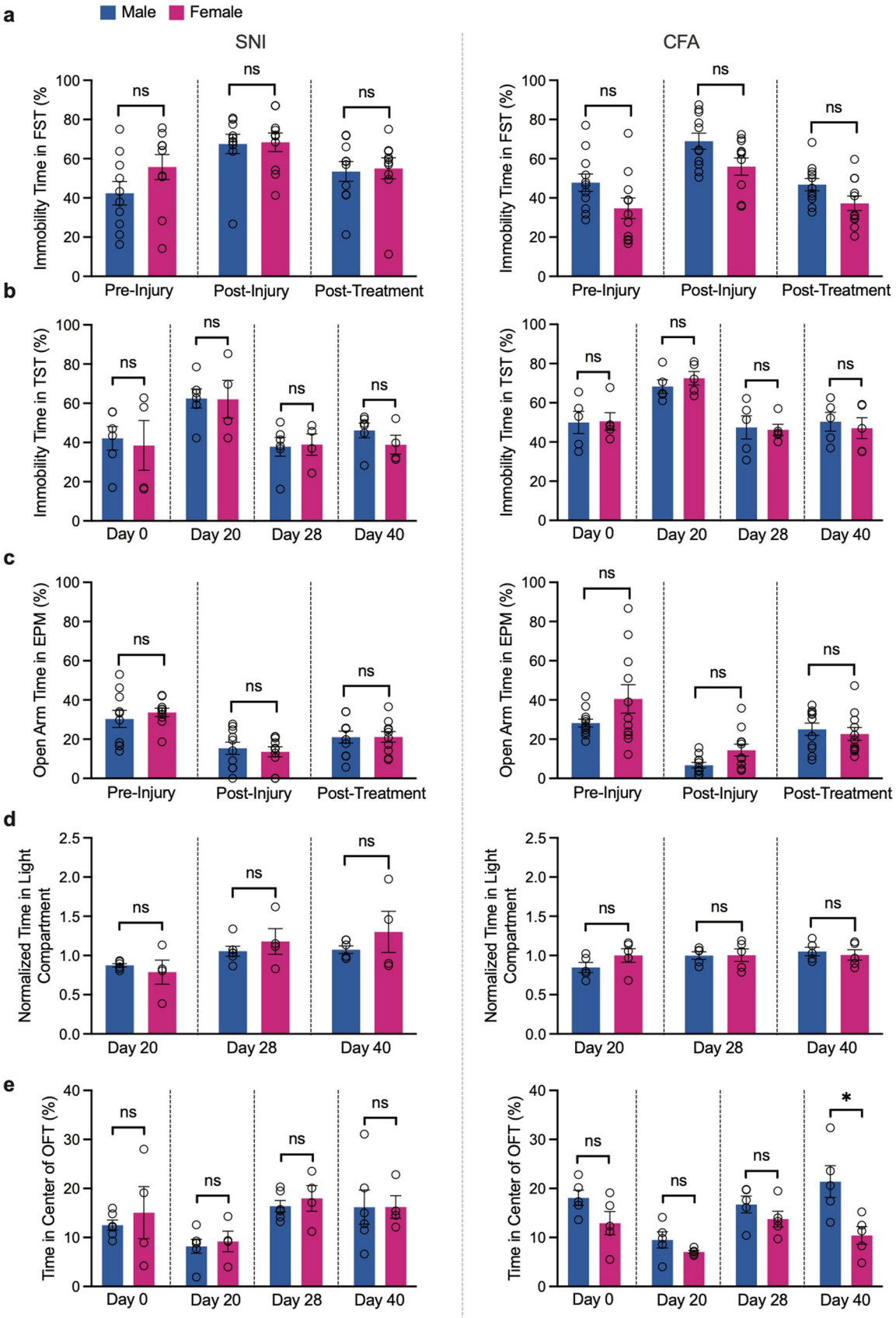

Extended Data Fig. 3 | See next page for caption.

https://doi.org/10.1038/s41593-025-02068-0

Extended Data Fig. 3 | Sex-specific mood-related behavioral responses in SNI and CFA mice. a, FST immobility time for SNI (left) and CFA (right) males (SNI: $n = 10$; CFA: $n = 11$) and females. (SNI: $n = 10$; CFA: $n = 11$). No significant differences were found pre-injury (SNI: $P = 0.296$; CFA: $P = 0.274$), post-injury (SNI: $P > 0.999$; CFA: $P = 0.419$), and post-treatment (SNI: $P > 0.999$; CFA: $P = 0.446$). **b**, TST immobility time for SNI (left) and CFA (right) males (SNI: $n = 6$; CFA: $n = 5$) and females (SNI: $n = 4$; CFA: $n = 5$). No significant differences were found on day 0 (SNI: $P > 0.999$; CFA: $P > 0.999$), 20 (SNI: $P > 0.999$; CFA: $P > 0.999$), 28 (SNI: $P > 0.999$; CFA: $P > 0.999$), and 40 (SNI: $P > 0.999$; CFA: $P > 0.999$). **c**, EPM open arm time for SNI (left) and CFA (right) males (SNI: $n = 10$; CFA: $n = 11$) and females (SNI: $n = 10$; CFA: $n = 11$). No significant differences were found pre-injury (SNI: $P = 0.755$; CFA: $P > 0.999$), post-injury (SNI: $P > 0.999$; CFA: $P = 0.344$), and post-treatment (SNI: $P > 0.999$; CFA: $P > 0.999$). **d**, Time in light compartment of light/dark box test for SNI (left) and CFA (right) males (SNI: $n = 6$; CFA: $n = 5$) and females (SNI: $n = 4$; CFA: $n = 5$). No significant differences were found on day 20 (SNI: $P > 0.999$; CFA: $P = 0.235$), 28 (SNI: $P > 0.999$; CFA: $P > 0.999$), and 40 (SNI: $P > 0.999$; CFA: $P > 0.999$). **e**, Time in center of open field test for SNI (left) and CFA (right) males (SNI: $n = 6$; CFA: $n = 5$) and females (SNI: $n = 4$; CFA: $n = 5$). No significant differences were found on day 0 (SNI: $P > 0.999$; CFA: $P = 0.441$), 20 (SNI: $P > 0.999$; CFA: $P > 0.999$), 28 (SNI: $P > 0.999$; CFA: $P > 0.999$). CFA females displayed a significant reduction in OPT center time on day 40 compared to males, while no significant differences were found in SNI mice (SNI: $P > 0.999$; CFA: $P = 0.041$). Data are represented as mean ± s.e.m. $^*P < 0.05$, ns = not significant. Detailed statistics are reported in Supplementary Table 1,i.

https://doi.org/10.1038/s41593-025-02068-0

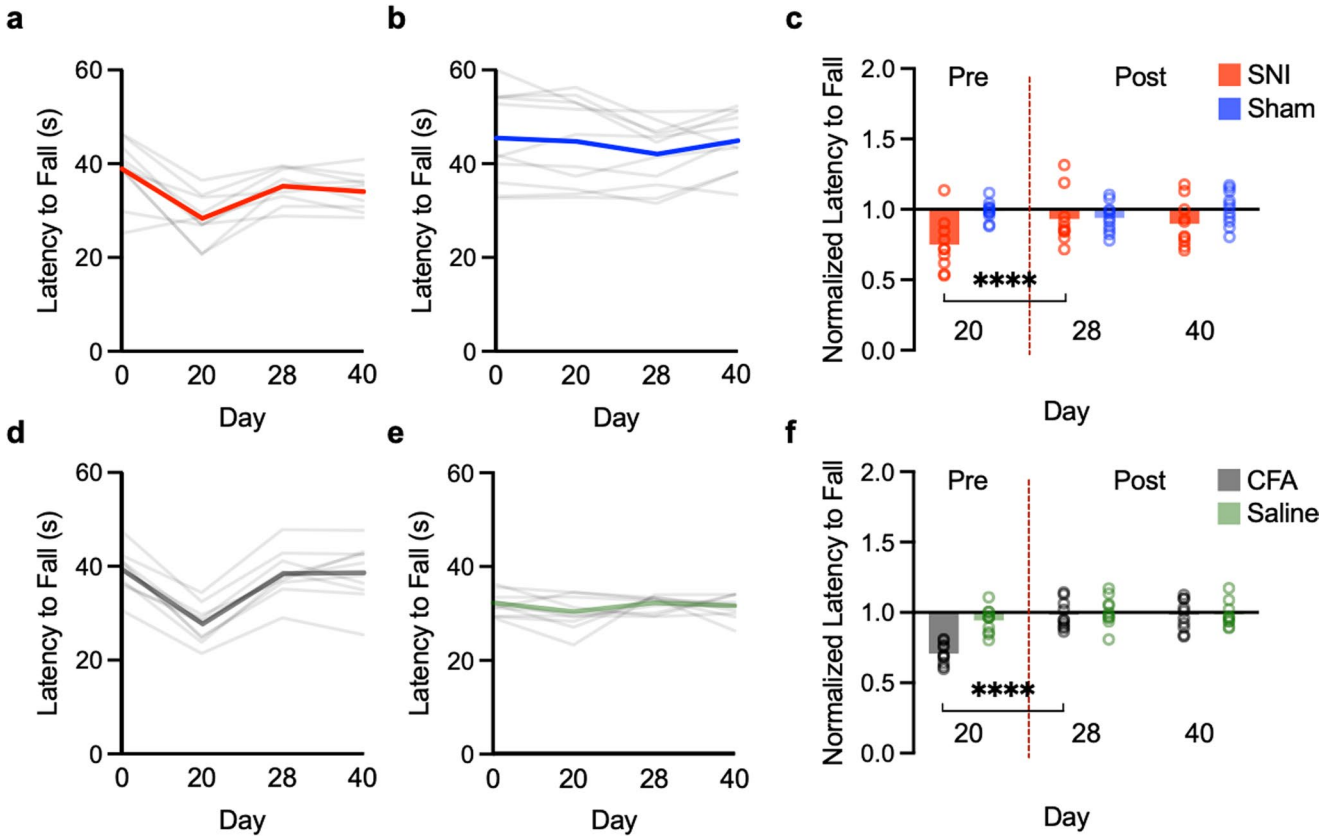

Extended Data Fig. 4 | Motor skill deficits induced by SNI and CFA interventions are reversed by psilocybin. a,**b**,**d**,**e**, Trajectory for latency to fall (seconds) for individual SNI (**a**, $n = 10$, red), sham (**b**, $n = 11$, blue), CFA (**d**, $n = 10$, gray) and saline (**e**, $n = 10$, green) animals over experimental timeline. Thicker line shows the population average. Motor performance declines at day 20, followed by a rapid recovery on day 28 following psilocybin injection. Sham and saline animals show consistent performance across all time points. **c**,**f**, Normalized latency to fall on an accelerating rotarod from baseline (day 0). Latency to fall decreases post-injury in (**c**) SNI ($n = 10$) and (**f**) CFA ($n = 10$) conditions, then increases post-psilocybin injection on day 28 (one-way ANOVA followed by Bonferroni's multiple comparisons test, SNI: $P = 7.9 \times 10^{-5}$, CFA: $P = 1.6 \times 10^{-8}$). Data are represented as mean. $^{****}P < 0.0001$. Detailed statistics are reported in Supplementary Table 1,j.

https://doi.org/10.1038/s41593-025-02068-0

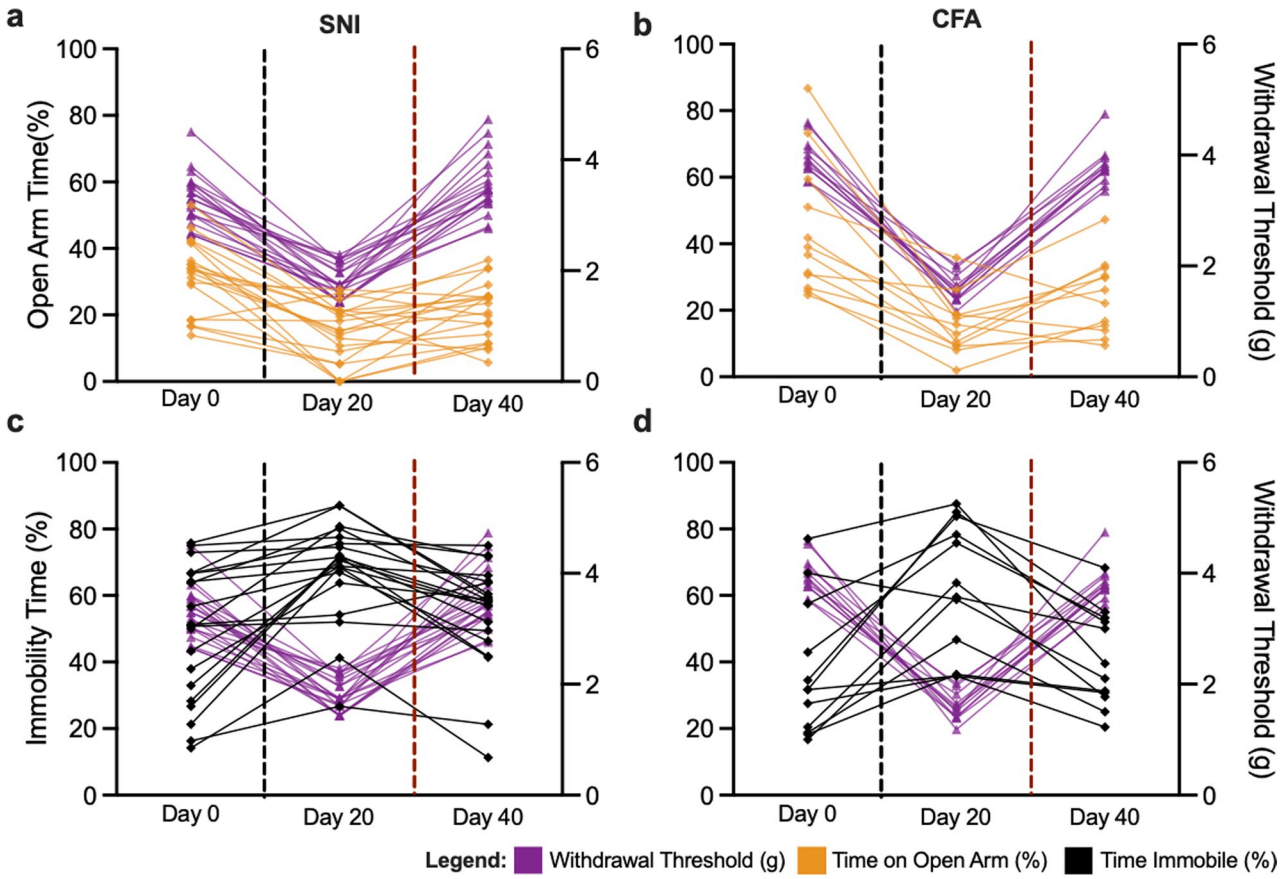

Extended Data Fig. 5 | Simultaneous tracking of mechanical hypersensitivity and mood dysfunction across individual mice in SNI and CFA conditions. **a**,**b**, Measurements of open arm activity in elevated plus maze (EPM) and withdrawal thresholds across multiple time points (day 0 (baseline); day 20 (post-injury); day 40 (after psilocybin treatment)) in individual (**a**) SNI ($n = 20$) and (**b**) CFA ($n = 22$) mice. **c**,**d**, Measurements of immobility time in forced swim test (FST) and withdrawal thresholds across multiple time points in individual (**c**) SNI ($n = 20$) and (**d**) CFA ($n = 22$) mice.

https://doi.org/10.1038/s41593-025-02068-0

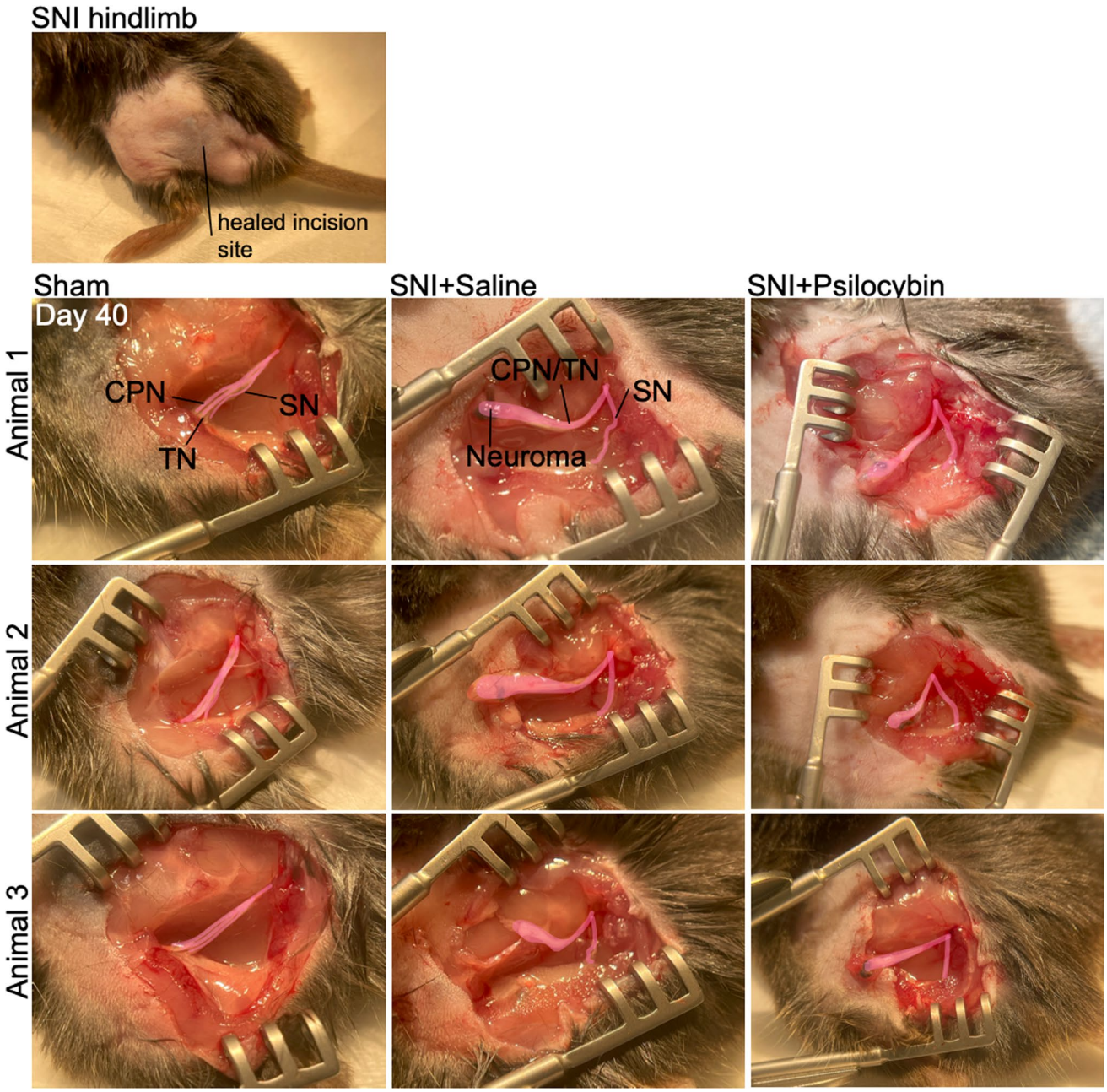

Extended Data Fig. 6 | Psilocybin treatment does not regenerate previous severed peripheral sciatic nerves. Top, photograph of SNI (left) location showing healed surgical site at level of skin. Bottom, representative photographs of sciatic nerve exposure in 3 sham (left) and 3 SNI (right) mice at day 40. SNI procedure results in a neuroma (isolated with blunt dissection) consisting of the common peroneal nerve (CPN) and tibial nerve (TN), while SN remains in normal position intact. Psilocybin treatment at day 28 in SNI mice (3 examples shown) does not induce any gross changes in the appearance of neuroma.

https://doi.org/10.1038/s41593-025-02068-0

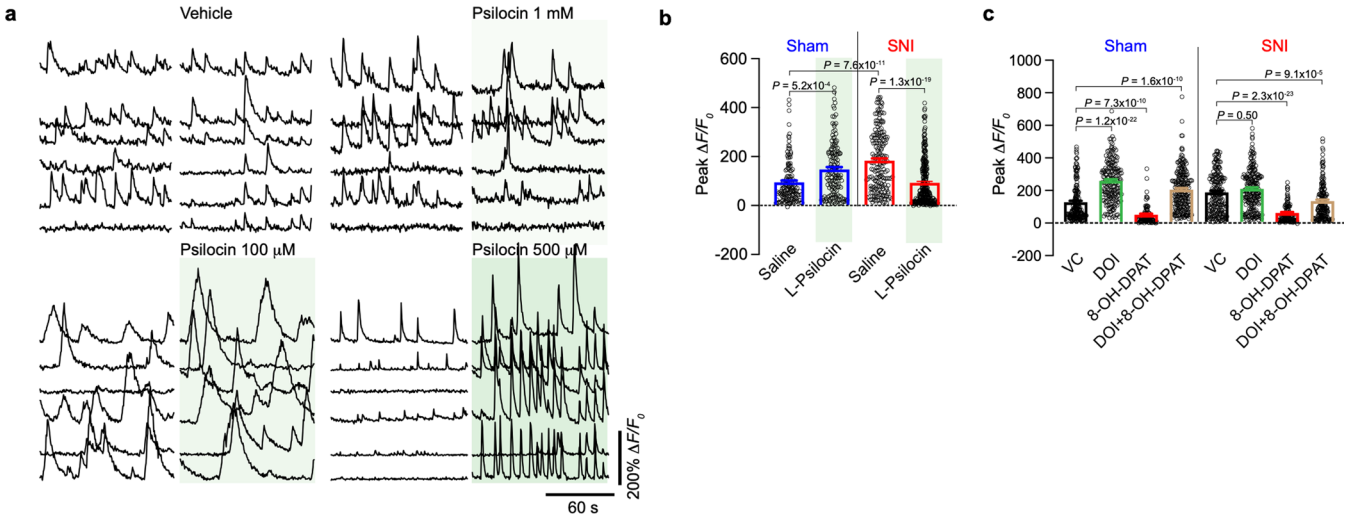

Extended Data Fig. 7 | L2/3 neuronal activity changes induced by local serotonergic receptor modulation in ACC. a, Representative GCaMP6f traces of individual neurons under wakefulness and following local (L-) psilocin (green-shaded area) at different doses (0 µM, 1 µM, 100 µM, 500 µM). Summary shown in Fig. 4h. **b**, L2/3 peak calcium responses in sham and SNI mice following saline and L-psilocin (200 µM; sham saline, $n = 143$ from 3 mice; sham L-psilocin, $n = 144$ from 3 mice; SNI sham, $n = 194$ from 3 mice; SNI L-psilocin, $n = 276$ from 4 mice). SNI condition increased the L2/3 peak responses compared to sham, which was reversed by L-psilocin (one-sided Kruskal–Wallis (98), $P = 3.4 \times 10^{-21}$ followed by Dunn's multiple comparison: sham versus SNI, $P = 7.6 \times 10^{-11}$; sham saline versus sham L-psilocin, $P = 5.2 \times 10^{-4}$, SNI saline versus SNI L-psilocin, $P = 1.3 \times 10^{-19}$). **c**, L2/3 peak calcium responses in sham and SNI mice following vehicle control (saline) and local application of DOI (sham $n = 189$ from 4 mice, SNI $n = 222$ from 4 mice), 8-OH-DPAT (sham $n = 100$ from 3 mice, SNI $n = 126$ from 3 mice), or DOI + 8-OH-DPAT (sham $n = 224$ from 5 mice, SNI $n = 171$ from 5 mice). Drug concentration was 200 µM for each condition; one-sided Kruskal–Wallis (430), $P = 9.3 \times 10^{-89}$ followed by Dunn's multiple comparisons shown in **c**. Data are represented as mean ± s.e.m in **b**,**c**.

https://doi.org/10.1038/s41593-025-02068-0

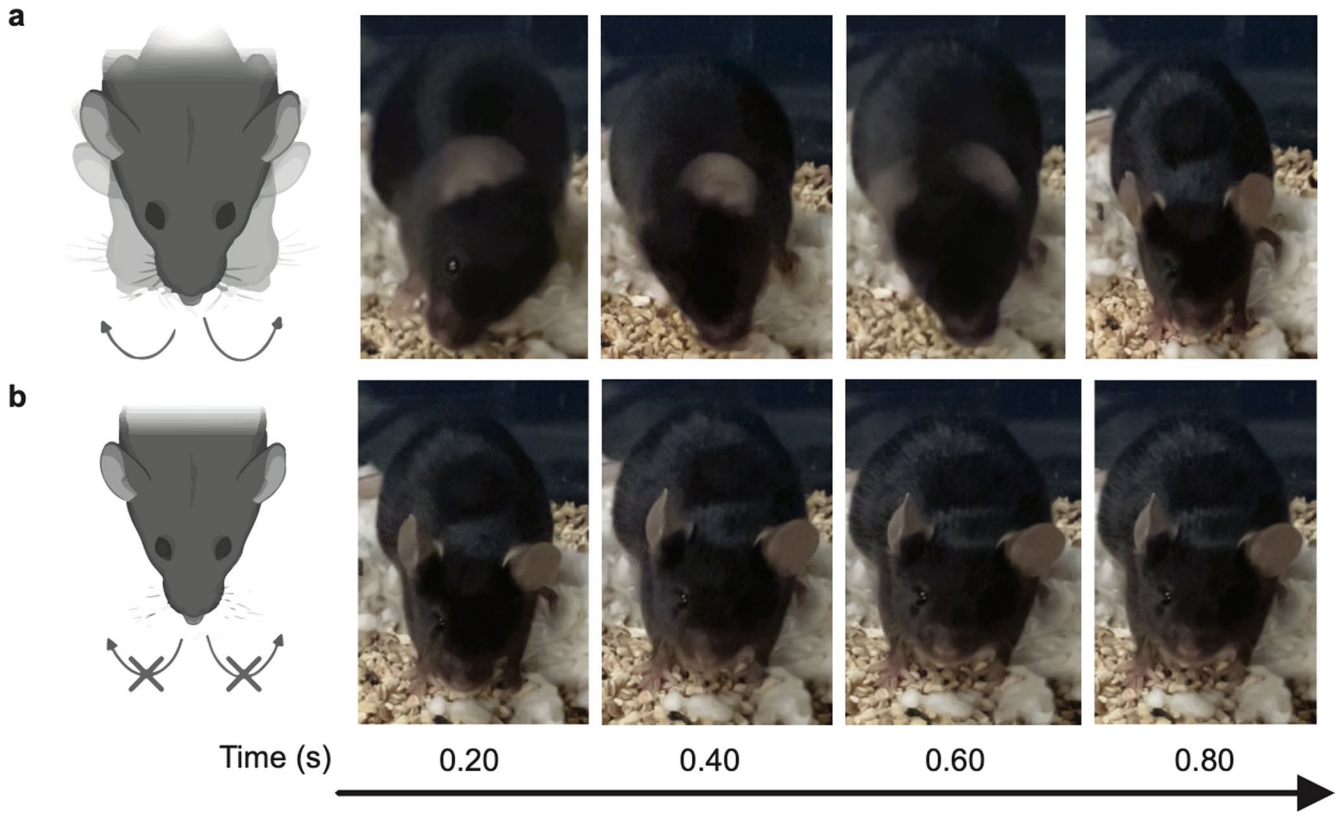

Extended Data Fig. 8 | Pretreatment with pimavanserin before psilocybin blocks the rotational head-twitch response. a,**b**, Psilocybin injection (**a**) induces the prototypical rotational 'wet-dog' head-twitch response, which was blocked by pimavanserin administration (**b**) before psilocybin. The cartoons in **a** and **b** (left) are created with BioRender.com.

https://doi.org/10.1038/s41593-025-02068-0

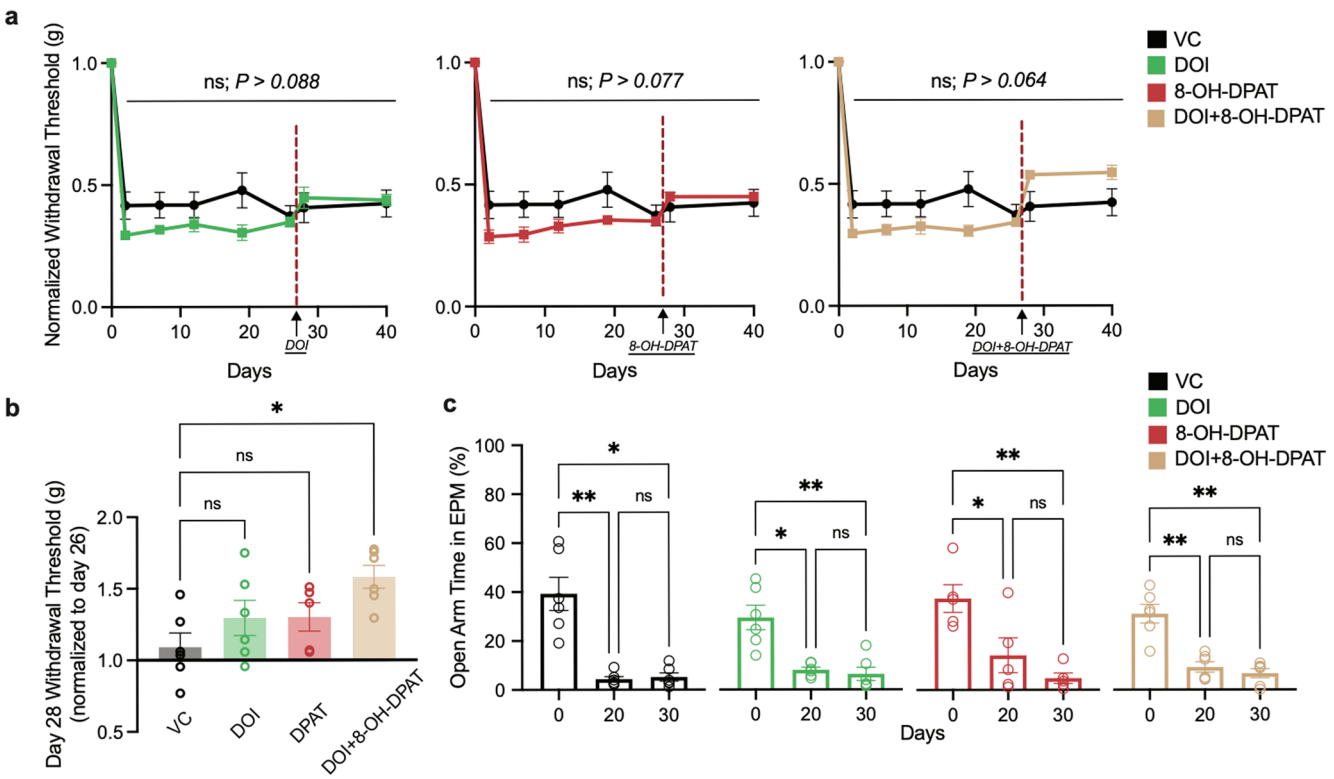

Extended Data Fig. 9 | Pharmacological activation of 5-HT$_{2A}$ and 5-HT$_{1A}$ receptors, individually or in combination, affects mechanical withdrawal thresholds and mood behavioral responses. a, Normalized hindlimb withdrawal thresholds (g) in SNI mice across different conditions. No difference is observed in DOI ($n = 6$), 8-OH-DPAT ($n = 5$), DOI + 8-OH-DPAT ($n = 6$) groups compared to vehicle controls ($n = 6$) (DOI: $P > 0.088$, 8-OH-DPAT: $P > 0.077$, DOI + 8-OH-DPAT: $P > 0.064$). **b**, Comparison of hindlimb withdrawal thresholds measured at day 28 normalized to day 26 across different treatment groups. A slight but significant improvement in withdrawal threshold was observed in the DOI + 8-OH-DPAT group compared to the VC group ($n = 6$, $P = 0.0157$). However, no significant improvement was observed in the DOI ($n = 6$, $P = 0.9985$) or 8-OH-DPAT ($n = 5$, $P > 0.999$) groups compared to VC. **c**, EPM open arm (%) pre-injury, post-injury, and post-treatment. No statistically significant improvement is observed in performance on the EPM post-injection across all drug groups. Data are presented as mean ± s.e.m. $^{**}P < 0.01$, $^{*}P < 0.05$, ns, non-significant. Detailed statistics are reported in Supplementary Table 1,k.

nature portfolio

Corresponding author(s): Cichon

Last updated by author(s): 8/19/2025

Reporting Summary

Nature Portfolio wishes to improve the reproducibility of the work that we publish. This form provides structure for consistency and transparency in reporting. For further information on Nature Portfolio policies, see our Editorial Policies and the Editorial Policy Checklist.

Statistics

For all statistical analyses, confirm that the following items are present in the figure legend, table legend, main text, or Methods section.

n/a	Confirmed	
☐	☒	The exact sample size (*n*) for each experimental group/condition, given as a discrete number and unit of measurement
☐	☒	A statement on whether measurements were taken from distinct samples or whether the same sample was measured repeatedly
☐	☒	The statistical test(s) used AND whether they are one- or two-sided *Only common tests should be described solely by name; describe more complex techniques in the Methods section.*
☒	☐	A description of all covariates tested
☐	☒	A description of any assumptions or corrections, such as tests of normality and adjustment for multiple comparisons
☐	☒	A full description of the statistical parameters including central tendency (e.g. means) or other basic estimates (e.g. regression coefficient) AND variation (e.g. standard deviation) or associated estimates of uncertainty (e.g. confidence intervals)
☐	☒	For null hypothesis testing, the test statistic (e.g. *F*, *t*, *r*) with confidence intervals, effect sizes, degrees of freedom and *P* value noted *Give P values as exact values whenever suitable.*
☒	☐	For Bayesian analysis, information on the choice of priors and Markov chain Monte Carlo settings
☒	☐	For hierarchical and complex designs, identification of the appropriate level for tests and full reporting of outcomes
☒	☐	Estimates of effect sizes (e.g. Cohen's *d*, Pearson's *r*), indicating how they were calculated

Our web collection on statistics for biologists contains articles on many of the points above.

Software and code

Policy information about availability of computer code

Data collection	Behavioral measurements of mechanical hypersensitivity were made with electronic von Frey Anesthesiometer (IITC Life Science). Withdrawal responses were recorded in triplicate for each hindlimb on each day of testing. Additionally forced swim, tail suspension, light/dark box, open field, elevated plus maze tests were conducted in custom constructed apparatuses. Conditioned place preference test was purchased from Maze Engineers. Behavioral time assessments were performed using video camera and AnyMaze software (Stoelting Co.) No code was used in collection of data. Two-photon images were collected on a Olympus RS DIY two-photon system (tuned to 920 nm) equipped with a Ti:Sapphire laser (Discovery, Coherent). Image acquisition was performed using FV10-ASW v.2.0 software and analyzed post hoc using NIH ImageJ software v.2.1.0.
Data analysis	ImageJ software v.2.1.0. for general image processing, Turbo Reg plugin in ImageJ v.2.1.0 for motion correction, Graph Pad Software v.9.3.1. for calcium analysis and behavioral testing.

For manuscripts utilizing custom algorithms or software that are central to the research but not yet described in published literature, software must be made available to editors and reviewers. We strongly encourage code deposition in a community repository (e.g. GitHub). See the Nature Portfolio guidelines for submitting code & software for further information.

Data

Policy information about availability of data

All manuscripts must include a data availability statement. This statement should provide the following information, where applicable:

- Accession codes, unique identifiers, or web links for publicly available datasets
- A description of any restrictions on data availability
- For clinical datasets or third party data, please ensure that the statement adheres to our policy

All data needed to evaluate the conclusions and replicate the figures presented in this article are provided in the source data and associated data will be available to the scientific community via FigShare (https://figshare.com/s/aae99484130e22266bbc).

Research involving human participants, their data, or biological material

Policy information about studies with human participants or human data. See also policy information about sex, gender (identity/presentation), and sexual orientation and race, ethnicity and racism.

Reporting on sex and gender	N/A
Reporting on race, ethnicity, or other socially relevant groupings	N/A
Population characteristics	N/A
Recruitment	N/A
Ethics oversight	N/A

Note that full information on the approval of the study protocol must also be provided in the manuscript.

Field-specific reporting

Please select the one below that is the best fit for your research. If you are not sure, read the appropriate sections before making your selection.

☒ Life sciences ☐ Behavioural & social sciences ☐ Ecological, evolutionary & environmental sciences

For a reference copy of the document with all sections, see nature.com/documents/nr-reporting-summary-flat.pdf

Life sciences study design

All studies must disclose on these points even when the disclosure is negative.

Sample size	No statistical tests were used to predetermine sample sizes, but the sample sizes for this study are similar to those generally employed in the field for behavioral testing.
Data exclusions	No animals were excluded from analysis.
Replication	Experiments were replicated in at least 3 separate litters of mice. Additionally, the effect of psilocybin was demonstrated in 2 different pain models.
Randomization	Animals were assigned to psilocybin or saline randomly.
Blinding	A.H. was blinded to treatment but not pain inducing procedures, as A.H. performed stated procedures.

Reporting for specific materials, systems and methods

We require information from authors about some types of materials, experimental systems and methods used in many studies. Here, indicate whether each material, system or method listed is relevant to your study. If you are not sure if a list item applies to your research, read the appropriate section before selecting a response.

Materials & experimental systems

n/a	Involved in the study
☐	☒ Antibodies
☒	☐ Eukaryotic cell lines
☒	☐ Palaeontology and archaeology
☐	☒ Animals and other organisms
☒	☐ Clinical data
☒	☐ Dual use research of concern
☒	☐ Plants

Methods

n/a	Involved in the study
☒	☐ ChIP-seq
☒	☐ Flow cytometry
☒	☐ MRI-based neuroimaging

Antibodies

Antibodies used

Primary cFos antibody solution (Cat # RPCA-c-FOS; EnCor Biotechnology; 1:1000 rabbit polyclonal) and a secondary Alexa-Fluor 568 goat anti-rabbit antibody solution (Cat # A-11011; Invitrogen by ThermoFisher Scientific; 1:300) were used.

Validation

The RPCA-c-FOS antibody was made against recombinant full length human c-FOS expressed in and purified from E. coli. It can be used to identify activated cells in cell culture and in sectioned material and to follow c-FOS expression using western blots of cell and tissue homogenates. Company documents that the antibody works well not only for western blotting, IF and ICC but also on formalin fixed paraffin embedded sections of human and rodent tissues. The same immunogen was used to generate a very popular mouse monoclonal antibody to c-FOS, MCA-2H2, and MCA-1B62, antibodies with similar properties.

Animals and other research organisms

Policy information about studies involving animals; ARRIVE guidelines recommended for reporting animal research, and Sex and Gender in Research

Laboratory animals

All mice were maintained at the University of Penn, Perelman School of Medicine, John Morgan animal facility under normal dark/light cycle conditions with controlled room temperature and humidity. Animals had access to free food and water. All animal handling was in accordance with guidelines set forth by the School of Medicine's Insitutional Animal Care and Use Committee (IACUC), approved protocol number: 807237. C57BL/6J mice at 2 months of age, using both sexes, were used for behavior tests and imaging.

Wild animals

No wild animals were used in this study.

Reporting on sex

Males and females were used in this study. Analysis of sex differences showed similar effect on mechanical hypersensitivity and axiodepressive-like behaviors.

Field-collected samples

No field collected sampled were used in this study.

Ethics oversight

Institutional Animal Care and Use Committee, University of Pennsylvania.

Note that full information on the approval of the study protocol must also be provided in the manuscript.

Plants

Seed stocks

N/A

Novel plant genotypes

N/A

Authentication

N/A